Bioorg. Med. Chem. 37 (2021) 116093

Contents lists available at ScienceDirect

Bioorganic & Medicinal Chemistry

journal homepage: www.elsevier.com/locate/bmc

# Discovery of 6-substituted thieno[2,3-*d*]pyrimidine analogs as dual inhibitors of glycinamide ribonucleotide formyltransferase and 5-aminoimidazole-4-carboxamide ribonucleotide formyltransferase in *de novo* purine nucleotide biosynthesis in folate receptor expressing human tumors

Adrianne Wallace-Povirk [b,1], Nian Tong [a,1], Jennifer Wong-Roushar [d,1], Carrie O'Connor [b], Xilin Zhou [a], Zhanjun Hou [b,c], Xun Bao [b], Gloria E. Garcia [d], Jing Li [b,c], Seongho Kim [b,c], Charles E. Dann III [d,*], Larry H. Matherly [b,c,*], Aleem Gangjee [a,*]

[a] *Division of Medicinal Chemistry, Graduate School of Pharmaceutical Sciences, Duquesne University, Pittsburgh, PA 15282, United States*
[b] *Department of Oncology, Wayne State University School of Medicine, Detroit, MI 48201, United States*
[c] *Barbara Ann Karmanos Cancer Institute, Detroit, MI 48201, United States*
[d] *Department of Chemistry, Indiana University, Bloomington, IN 47405, United States*

A B S T R A C T

We discovered 6-substituted thieno[2,3-*d*]pyrimidine compounds (**3**–**9**) with 3–4 bridge carbons and side-chain thiophene or furan rings for dual targeting one-carbon (C1) metabolism in folate receptor- (FR) expressing cancers. Synthesis involved nine steps starting from the bromo-aryl carboxylate. From patterns of growth inhibition toward Chinese hamster ovary cells expressing FRα or FRβ, the proton-coupled folate transporter or reduced folate carrier, specificity for uptake by FRs was confirmed. Anti-proliferative activities were demonstrated toward FRα-expressing KB tumor cells and NCI-IGROV1 ovarian cancer cells. Inhibition of *de novo* purine biosynthesis at both 5-aminoimidazole-4-carboxamide ribonucleotide formyltransferase and glycinamide ribonucleotide formyltransferase (GARFTase) was confirmed by metabolite rescue, metabolomics and enzyme assays. X-ray crystallographic structures were obtained with compounds **3**–**5** and human GARFTase. Our studies identify first-in-class C1 inhibitors with selective uptake by FRs and dual inhibition of enzyme targets in *de novo* purine biosynthesis, resulting in anti-tumor activity. This series affords an exciting new platform for selective multi-targeted anti-tumor agents.

## 1. Introduction

One-carbon (C1) metabolism continues to be of considerable interest, reflecting the biological importance of folates in the generation of thymidylate, purines, serine, and methionine, and the role of S-adenosylmethionine in the methylation of DNA and proteins.[1,2] Recent studies have revealed new and intriguing roles for C1 metabolism, including those involving inflammatory responses elicited by macrophages[3] and a host of mitochondrial functions ranging from redox regulation and glutathione biosynthesis to oxidative phosphorylation.[4-6]

C1 inhibitors have been used for cancer therapy for decades, beginning with the discovery of aminopterin in the 1940s.[8] Previous C1 inhibitors focused on targeting thymidylate synthase (TS) and dihydrofolate reductase (DHFR), typified by pemetrexed (PMX) and methotrexate (MTX), respectively[9,10] (Figure 1). While these inhibitors continue to find clinical use for diseases including non-small cell lung

*Abbreviations:* ATP, Adenosine triphosphate; ADP, adenosine diphosphate; AMP, adenosine monophosphate; AICA, 5-aminoimidazole-4-carboxamide; ZMP, 5-aminoimidazole-4-carboxamide ribonucleotide; AICARFTase, 5-aminoimidazole-4-carboxamide ribonucleotide formyltransferase; AMPK, AMP-activated protein kinase; ATIC, AICARFTase/inosine monophosphate cyclohydrolase; CHO, Chinese hamster ovary; EOC, epithelial ovarian cancer; FBS, fetal bovine serum; DMEM, Dulbecco's minimal essential medium; DHFR, dihydrofolate reductase; DPBS, Dulbecco's phosphate-buffered saline; FAICAR, formyl 5-aminoimidazole-4-carboxamide ribonucleotide; FF RPMI, folate-free RPMI 1640; FR, folate receptor; 10-CHO-THF, N10-formyl tetrahydrofolate; fGAR, formyl glycinamide ribonucleotide; GAR, glycinamide ribonucleotide; GARFTase, glycinamide ribonucleotide formyltransferase; HBSS, Hank's balanced salts solution; HBS, HEPES-buffered saline; IMP, inosine monophosphate; MTX, methotrexate; MEM, minimal essential media; C1, one-carbon; PMX, pemetrexed; PEG, polyethylene glycol; PDX, pralatrexate; PCFT, proton-coupled folate transporter; RTX, raltitrexed; RFC, reduced folate carrier; TLC, thin layer chromatography; TS, thymidylate synthase; TCA, trichloroacetic acid; TCEP, Tris(2-carboxyethyl)phosphine.

* Corresponding authors at: Department of Oncology, Wayne State University School of Medicine, Detroit, MI 48201, United States (L. Matherly).
*E-mail addresses:* cedann@indiana.edu (C.E. Dann), matherly@karmanos.org (L.H. Matherly), gangjee@duq.edu (A. Gangjee).

[1] These authors contributed equally to this work.

https://doi.org/10.1016/j.bmc.2021.116093
Received 17 November 2020; Received in revised form 16 February 2021; Accepted 19 February 2021
Available online 26 February 2021

cancer, malignant pleural mesothelioma and hematologic malignancies,[8] they are plagued by toxicities due to their lack of tumor selectivity and by acquired or innate drug resistance, reflecting altered expression of target enzymes, decreased membrane transport and loss of polyglutamylation.[11]

Reflecting their ionic nature, folates cannot diffuse into cells and must be actively transported. To accommodate this limitation, three key transporters of folates and related compounds have evolved in mammalian cells. The reduced folate carrier (RFC) is responsible for the majority of cellular folate uptake.[12] This anion antiporter is expressed in both normal and cancerous tissues.[12] The proton-coupled folate transporter (PCFT) represents another critical transporter for folates[13] as it is highly expressed on the apical brush border of the proximal duodenum and jejunum where its main function involves the absorption of dietary folates.[14] PCFT is a proton/folate symporter and operates best at acidic pH.[13] Expression of PCFT has been reported in a wide range of solid tumors, including epithelial ovarian cancer (EOC), lung adenocarcinoma and malignant pleural mesothelioma.[15-19] Folate receptor (FR) α and FRβ also contribute to the uptake of folates and related compounds via an endocytotic mechanism.[20,21] FRα is expressed in normal epithelial tissues, including proximal tubules of the kidney, choroid plexus and placenta, whereas FRβ is expressed in hematopoietic tissues and activated macrophages, including tumor-associated macrophages.[21,22] In relation to cancer, substantial levels of FRα are detected in EOC, with lower levels in lung adenocarcinoma, uterine cancer, and triple negative breast cancer.[21,23,24,25]

In tumors, FRα gains access to the circulation by switching from an apical to a non-polarized pattern of expression.[20] In principle, this provides a means for FRα-targeted therapies to achieve tumor specificity, as access to FRα from the circulation would be spared in normal epithelial cells that express FRα. With potential for tumor selectivity, several FRα-targeted therapies have been developed and advanced to clinical trials. Clinically tested FRα-targeted therapies include a FRα monoclonal antibody (Farletuzumab; Morphotech),[26] a FRα-targeted antibody-drug conjugate (IMGN853; ImmunoGen),[27] folic acid-drug conjugates (Vintafolide, EC1456, EC1788)[28] and a FR-targeted antifolate (ONX-0801; Onyx Therapeutics).[29] ImmunoGen's FRα-targeting antibody-drug conjugate (IMGN853) was advanced to phase III clinical trials and showed efficacy as a single agent in patients whose tumors expressed high levels of FRα. IMGN853 is currently being tested in combination regimens for both platinum sensitive and resistant cancers in a Phase 1b clinical trial.[27,30] ONX-0801 is a TS inhibitor that showed promising phase 1 clinical results with multiple partial responses and is being advanced to phase 2 clinical trials.[29]

PMX, an iconic C1 inhibitor, is a 5-substituted pyrrolo[2,3-*d*]pyrimidine with a 2-carbon bridge which is linked to a *p*-aminobenzoyl-L-glutamate (Figure 1).[10] PMX is primarily transported by RFC and PCFT.[31] The principal intracellular target for PMX is TS, as noted above, with secondary inhibition at other cytosolic targets including 5-aminoimidazole-4-carboxamide (AICA) ribonucleotide formyltransferase (AICARFTase) and glycinamide ribonucleotide formyltransferase (GARFTase) in *de novo* purine biosynthesis, and DHFR.[10,32]

We previously described 6-substituted pyrrolo[2,3-*d*]pyrimidine compounds (e.g., **AGF23** in Figure 1) with modifications in the length and nature of the bridge, and variations of the aromatic ring (phenyl, thienophene, pyridine) in the side-chain.[7, 33–39] All compounds were GARFTase inhibitors and showed uptake into tumor cells via FRs and PCFT. However, selectivity for FRs and PCFT could be incomplete with additional uptake by a non-mediated process.[7,36]

In an effort to improve transport selectivity for our targeted pyrrolo[2,3-*d*]pyrimidine agents,[7] we replaced the pyrrole in **AGF23** with a thiophene to generate 6-substituted thieno[2,3-*d*]pyrimidine benzoyl analogs typified by compounds **1** (3-carbon bridge) and **2** (4-carbon bridge) (Figure 2).[40] Isosteric replacement of the pyrrole with a thiophene ring results in an increased ring size that more closely approximates the 6–6 fused pteridine ring system of the natural folate cofactor.[40] Further, replacement of the NH of the pyrrole with an S examines the relative importance of a hydrogen bond donor (NH) versus a hydrogen bond acceptor (S) in relation to biological activity. Both **1** and **2** were potent and selective inhibitors of proliferation toward cells that express FRα or FRβ. These analogs are distinct from previous pyrrolo[2,3-*d*]pyrimidine inhibitors[7,33–39] and clinically used classical

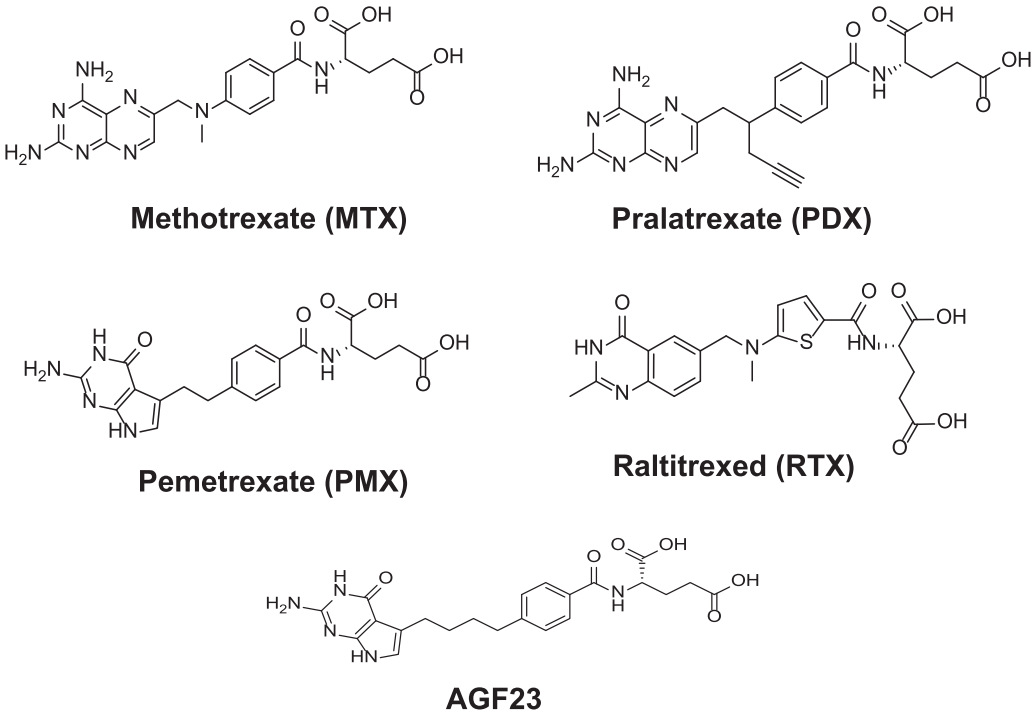


**Figure 1.** Structures of classic antifolate drugs, including methotrexate (MTX), pemetrexed (PMX), pralatrexate (PDX), and raltitrexed (RTX), along with the 6-pyrrolo[2,3-*d*]pyrimidine antifolate **AGF23.**[7]

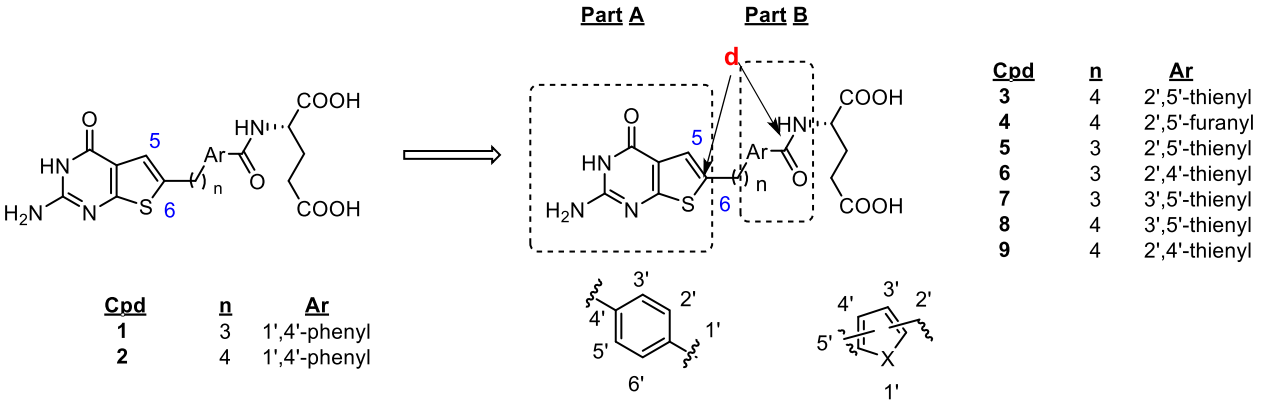


**Figure 2.** Structures of 6-substituted thieno[2,3-*d*]pyrimidine analogs **1**–**9**. For discussion of docked ligands herein, the distance (**d**) between the 6-position of the bicyclic aryl system (Part A) and the carbonyl carbon of the L-glutamate (Part B) are noted (Table 1).

antifolates, including PMX (pyrrolo[2,3-*d*]pyrimidine), raltitrexed (RTX) (quinazoline), and pralatrexate (PDX) and MTX (both pteridines) (Figure 1), in that they are neither substrates for RFC nor PCFT.[40] While compounds **1** and **2** were inhibitors of GARFTase, from patterns of metabolite "rescue", a secondary target (i.e., AICARFTase) was implied but not definitively established.[40]

The importance of multi-target inhibition in cancer chemotherapy is well documented.[41,42] Combination chemotherapy has the advantage in that it delays or circumvents the development of drug resistance.[42-46] Since the predominant reason for cancer chemotherapy failure is the development of drug resistance, compounds capable of inhibiting more than one target would similarly afford the benefits of drug combinations.[42-46] In the event that these multi-targeted agents also possess tumor-selective transport, multi-targeted tumor-selective agents would be at hand.

Based on these considerations, we further explored the identity of the putative second intracellular target in *de novo* purine biosynthesis for the thieno[2,3-*d*]pyrimidine inhibitors.[40] We selected the most potent analog **2**[40] and identified it as a GARFTase and AICARFTase inhibitor in isolated enzyme assays to accompany its FRα selectivity, providing impetus to further examine a broader series of thieno[2,3-*d*]pyrimidines as selective FR-targeted antitumor agents. To investigate the structural requirements for selective FR targeting and inhibition of dual C1 pathways at GARFTase and AICARFTase, we designed, synthesized and evaluated thieno[2,3-*d*]pyrimidine compounds **3**–**9** (Figure 2) with 3- or 4- atom bridge lengths and isosteric aryl replacements of the side-chain phenyl ring of **2**, including positional thiophene regioisomers and a furan. Unlike the side-chain benzene in compound **2**, the thiophene and furan replacements in **3**–**9** afford electron-rich heterocycles[47] with electron-donating heteroatoms. This, combined with differing distances between the bicyclic thieno[2,3-*d*]pyrimidine scaffold (part A) and the L-glutamate (part B) (Figure 2; Table 1), allow for distinct bound conformations, thus additional interactions with target proteins (i.e., transporter(s) and target enzyme(s)) that may not possible for the side-chain benzene compounds.

In this report, we present the synthesis and structure–activity studies for the expanded 6-substituted thieno[2,3-*d*]pyrimidine series as we explore the potential of these compounds as multi-targeted tumor selective agents. We document the biological impact of these novel analogs, including their mechanisms of cellular uptake, and we comprehensively establish their intracellular enzyme targets and metabolic effects. For compounds **3**–**5**, we also report X-ray crystal structures with human GARFTase.

## 2. Rationale for proposed compounds: Molecular modeling

Based on our finding that the FR-selective 6-substituted thieno[2,3-*d*]pyrimidines typified by compound **2** were inhibitors of *de novo* purine biosynthesis at GARFTase, with possible dual inhibition of AICARFTase,[40] we evaluated **2** as an inhibitor in *in vitro* assays with purified human GARFTase and AICARFTase. As previously reported,[40] compound **2** inhibited GARFTase (Ki of 2.97 μM) and AICARFTase/IMP cyclohydrolase (ATIC)[4] (Ki of 9.48 μM) (Table 3). This establishes that the thieno[2,3-*d*]pyrimidine scaffold affords both FR selectivity[40] and dual inhibition at GARFTase and AICARFTase. These unique attributes of **2** provided strong impetus for further exploration of thieno[2,3-*d*]pyrimidines as selective targeted antitumor agents.

To provide rationale for our proposed thieno[2,3-*d*]pyrimidine analogs, we carried out molecular modeling studies of the lead compound **2** and compounds **3**–**9** with 3- or 4- atom bridge lengths and positional thiophene regioisomers and a furan (Figure 2). The binding modes were generated using X-ray crystal structures of human FRα (5IZQ),[48] FRβ

**Table 1**
Properties of 6-substituted thieno[2,3-*d*]pyrimidine compounds and docked scores in FRα, FRβ, GARFTase and AICARFTase.

| Compound | n | Distance in energy minimized conformation (Å) | FRα (kcal/mol) | FRβ (kcal/mol) | GARFTase (kcal/mol) | AICARFTase(kcal/mol) |
|---|---|---|---|---|---|---|
| **2** | 4 | 10.47 | −15.40 | −14.90 | −15.02 | −12.91 |
| **3** | 4 | 8.36 | −15.67 | −15.45 | −14.82 | −12.54 |
| **4** | 4 | 6.66 | −15.06 | −13.94 | −15.83 | −12.21 |
| **5** | 3 | 8.30 | −15.42 | −15.48 | −15.26 | −13.09 |
| **6** | 3 | 7.18 | −14.90 | −14.01 | −15.99 | −13.08 |
| **7** | 3 | 7.44 | −14.38 | −14.60 | −16.26 | −13.08 |
| **8** | 4 | 9.84 | −15.19 | −14.99 | −15.10 | −12.99 |
| **9** | 4 | 7.66 | −15.98 | −14.97 | −15.85 | −12.93 |
| **PMX** | 2 | 8.09 | −14.20 | −13.28 | −14.45 | −11.36 |

The binding modes for the proposed compounds were generated with X-ray crystal structures of human FRα (5IZQ),[48] FRβ (4KN2),[49] GARFTase (4ZYW)[50,51] and AICARFTase (1P4R)[52] using an induced-fit docking protocol (Schrödinger LLC).[53] The distances between parts A and B for the different ring systems (Figure 2) are listed as those from the aryl 6 positional carbon on the thieno[2,3-*d*]pyrimidine (**2**–**9**) or pyrrolo[2,3-*d*]pyrimidine (for PMX) scaffold to the carbonyl carbon on the L-glutamate in the energy-minimized conformations.

**Table 2**
$IC_{50}$ (in nM) for 6-substituted thieno[2,3-*d*]pyrimidine analogs and classical antifolates in RFC-, PCFT- and FR-expressing cell lines.

| Compound | RFC | | FRα | FRβ | PCFT | RFC/FRα/PCFT | | | | |
|---|---|---|---|---|---|---|---|---|---|---|
| | PC43-10 | R2 | RT16 | D4 | R2/PCFT4 | KB | KB (+FA) | NCI-IGROV1 | NCI-IGROV1 (+FA) | Ade/Thd/AICA |
| **2** | >1000 | >1000 | 9 (2.9) | 20 (3.9) | >1000 | 4.9 (1.3) | >1000 | 5.9 (1.9) | >1000 | Ade |
| **3** | >1000 | >1000 | 2.55 (0.76) | 1.67 (0.67) | >1000 | 2.10 (0.20) | >1000 | 10.14 (0.62) | >1000 | Ade |
| **4** | >1000 | >1000 | 10.5 (2.85) | 2.6 (0.64) | >1000 | 7.9 (0.93) | >1000 | >1000 | >1000 | Ade |
| **5** | >1000 | >1000 | 0.34 (0.09) | 1.75 (0.17) | >1000 | 1.42 (0.48) | >1000 | 54.13 (19.20) | >1000 | Ade |
| **6** | >1000 | >1000 | 0.44 (0.04) | 0.24 (0.06) | 107.29 (38.76) | 1.48 (0.04) | >1000 | 86.70 (10.23) | >1000 | Ade |
| **7** | >1000 | >1000 | 1.08 (0.43) | 0.72 (0.21) | 80.45 (8.77) | 1.82 (0.06) | >1000 | 25.97 (8.03) | >1000 | Ade |
| **8** | >1000 | >1000 | 0.91 (0.11) | 1.21 (0.01) | >1000 | 4.74 (0.47) | >1000 | >1000 | >1000 | Ade |
| **9** | >1000 | >1000 | 5.62 (1.31) | 5.63 (1.63) | 460.21 (97.68) | 6.85 (0.99) | >1000 | 108.21 (28.20) | >1000 | Ade |
| **PMX** | 14 (205) | 258 (44) | 42 (9) | 60 (8) | 13.2 (2.4) | 68 (12) | 327 (103) | 102 (25) | 200 (18) | Thd/Ade |
| **MTX** | 12 (1.1) | 216 (9) | 114 (31) | 106 (11) | 121 (17) | 6.0 (0.6) | 20 (2.4) | 21 (3.4) | 22 (2.1) | Ade/Thd |

Proliferation assays were performed for CHO sublines engineered to express human RFC (PC43-10), FRα (RT16), FRβ (D4) or PCFT (R2/PCFT4), and transporter-null (R2) CHO cells,[7,40,54,56] and KB and NCI-IGROV1 human tumor cells (both express RFC, FRα, and PCFT). To measure FR-mediated drug delivery, experiments were performed in the presence or absence of 200 nM folic acid (+FA). Results are presented as $IC_{50}$ values, corresponding to the concentrations that inhibit growth by 50% relative to cells incubated without drug. The data are mean values from at least 3 experiments (+/- standard errors in parentheses). Data for MTX, PMX, and **2** have been previously published.[7,40] Results are summarized for KB cells for the protective effects of adenosine (Ade) (60 μM), thymidine (Thd) (10 μM), or 5-aminoimidazole-4-carboxamide (AICA) (320 μM). Detailed graphs of folic acid and nucleoside/AICA protection results are shown in Figure 7. Methods are summarized in the Experimental Section. Undefined abbreviations: Ade, adenosine; AICA, 5-aminoimidazole-4-carboxamide; FA, folic acid; ND, not determined; Thd, thymidine.

**Table 3**
$K_i$ values for inhibition of human GARFTase and AICARFTase by 6-substituted thieno[2,3-*d*]pyrimidine compounds.

| Compound | GARFTase $K_i$ (μM) | ATIC $K_i$ (μM) |
|---|---|---|
| **2** | 2.97 (0.85) | 9.48 (2.77) |
| **3** | 1.36 (0.63) | 5.15 (0.59) |
| **4** | 10.72 (2.74) | 24.71 (5.15) |
| **5** | 8.19 (3.22) | 14.46 (6.05) |
| **6** | 4.28 (1.06) | 19.84 (5.28) |
| **7** | 0.91 (0.43) | 8.37 (1.47) |
| **8** | 0.15 (0.05) | 1.07 (0.40) |
| **9** | >150 | 8.03 (2.70) |
| **MTX** | >150 | >200 |
| **PMX** | 5.19 (1.63) | 0.88 (0.56) |

GARFTase activity was determined by measuring formation of tetrahydrofolate from 10-formyl tetrahydrofolate (10-CHO-THF) using a spectrophotometric assay (298 nm) in the presence of the tested analogs. Detailed methods are described in the Experimental Section. Results are shown as mean values +/- standard errors from at least three replicate assays. The results for MTX and PMX were previously reported.[4,50]

(4KN2),[49] GARFTase (4ZYW)[50,51] and ATIC (1P4R)[52] and an induced-fit docking protocol (Schrödinger LLC)[53] to explore binding interactions and to validate drug targets. The best (lowest) docked scores for ligand binding are summarized in Table 1**.** The distances from the aryl 6-positional carbon on the thieno[2,3-*d*]pyrimidine scaffold (Part A) to the carbonyl carbon on the L-glutamate moiety (Part B) (Figure 2) in the energy minimized conformations were also determined for compounds **3**–**9** (Table 1).

The X-ray crystal structures of our previous compounds with human FRα (5IZQ)[48] and GARFTase (4ZYW),[50,51] and the computationally docked structures of our targeted molecules exhibited different conformational requirements for attachment to FRα and GARFTase. We reported[50, 51] that flexibility is essential for binding to both FRα (5IZQ)[48] and GARFTase (4ZYW).[50,51] The distances (Table 1) between parts A and B of our inhibitors are critical in providing the requisite flexibility to enable access to multiple cellular targets (FRα, FRβ, GARFTase and AICARFTase).[33] Thus, by varying the measured distances between the bicyclic thieno[2,3-*d*]pyrimidine scaffold and the L-glutamate moiety (e.g., compound **4** versus compound **8**), the binding affinities with target proteins (i.e., transporter(s) and target enzymes) could be manipulated to potentially afford better analogs than **2.**

For FRα (5IZQ),[48] all the 3C– and 4C-bridged compounds **3**–**9** with different aromatic ring side-chains showed excellent docked scores of −14.08 to −15.98 kcal/mol (Table 1). Docked poses in FRα for the lead compound **2** and the designed analogs **3** and **8** are shown as examples in Figure 3**A.** The thieno[2,3-*d*]pyrimidine of **3** and **8** aligns well with **2** in the FRα crystal structure. The bicyclic scaffolds form π–π stacking with Tyr85, whereas the 2-$NH_2$ of the scaffold forms hydrogen bonds with the side-chain carboxylate of Asp81 and the side-chain of Ser174, the 3-NH hydrogen bonds with the side-chain hydroxyl of Ser174 and the 4-oxo moiety interacts with the side-chain nitrogen of Arg103. The 5-member rings of **2, 3** and **8** show π–π stacking with the bicyclic ring with Trp171. The L-glutamates of **2, 3** and **8** are oriented by polar contacts of the α-carboxylates with the backbone amide of Gly137, the backbone amide of Trp138, and the indole nitrogen of Trp140. The γ-carboxylate forms a salt bridge with the side-chain of Lys136 and hydrogen bonds with the indole nitrogen of the side-chain of Trp102 and the side-chain of Lys136.

The docked poses of all the thieno[2,3-*d*]pyrimidine compounds **3**–**9** in FRβ exhibited similar trends as in FRα. Again, compounds **3**–**9** showed excellent docked scores (-13.94 to −15.48 kcal/mol) in FRβ (Table 1). Docked poses in FRβ for the lead compound **2** and designed analogs **3** and **8**, as examples, are shown in Figure 3**B.** Similar to **2** in FRβ**,** the bicyclic thieno[2,3-*d*]pyrimidine scaffolds of **3** and **8** have the same energetically favorable hydrogen bonds at Asp97, Arg119 and Ser190, and π–π stacking with the aromatic side-chains of Tyr101 and Trp187. The thiophene bridge compounds **3** and **8** have π–π stacking with Trp156, similar to compound **2.** Unlike the docked poses in FRα, the L-glutamate moieties of **3** and **8** occupy slightly different orientations compared to the corresponding L-glutamate of **2.** The α-carboxylate of **2** makes no interactions with protein atoms, and the γ-carboxylate of **2** forms a network of a salt bridge and hydrogen bonds with the side-chain of Arg152, the NH of Gln116 and the indole nitrogen of Trp118. By comparison, the α-carboxylates of **3** and **8** form networks of hydrogen bonds with the backbone of Gly153 and the indole nitrogen of the Trp156 side-chain, and the γ-carboxylates form similar interactions with Gln116, Trp118 and Arg152 as **2.**

We docked our designed thieno[2,3-*d*]pyrimidine analogs **3**–**9** in the crystal structure of human GARFTase (PDB 4ZYW).[50,51] All the compounds showed excellent docked scores of −14.82 to −16.26 kcal/mol, with compound **7** having the best docked score (Table 1). Docked poses for the lead compound **2** and designed analogs **3** and **7**, as examples, are shown in Figure 4. The docked poses of **3** and **7** indicate that the thieno[2,3–*d*]pyrimidine scaffolds for these compounds form the same interactions as **2.** However, replacement of the bridge phenyl by a 2′,5′-substituted thiophene affords compound **3,** which showed different interactions of the L-glutamate moiety. The α-carboxylates of **2, 3,** and **7** form the same salt bridge interactions with Arg871 and hydrogen bond

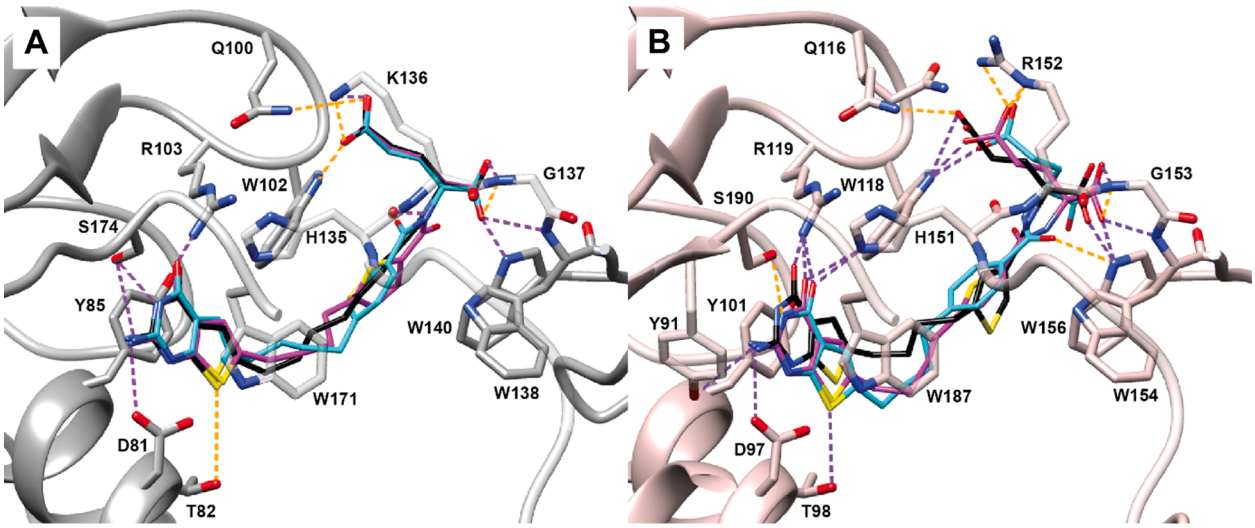


**Figure 3.** Molecular modeling studies of compounds **2, 3** and **8** in (A) human FRα (5IZQ)[48] and (B) human FRβ (4KN2).[49] **A.** Superimposition of the docked poses of **2** (cyan, −15.40 kcal/mol), **3** (magenta, −15.67 kcal/mol) and **8** (black, −15.19 kcal/mol) in FRα (5IZQ). **B.** Docked poses of **2** (cyan, −14.90 kcal /mol), **3** (magenta, −15.45 kcal /mol) and **8** (black, −14.99 kcal/mol) in human FRβ (4KN2). Polar contacts are depicted in dashed lines, where purple lines show conserved interactions between the crystal structure complexes and the docked models. Contacts shown as orange dashes are unique to docked models. For comparison, ligand contacts for the crystallographic starting models, 5IZQ and 4KN2, are provided in the Supporting Information (**Figure S1**). Induced-fit docking studies were performed and visualized using Maestro 12.3 (Schrödinger LLC).[53.]

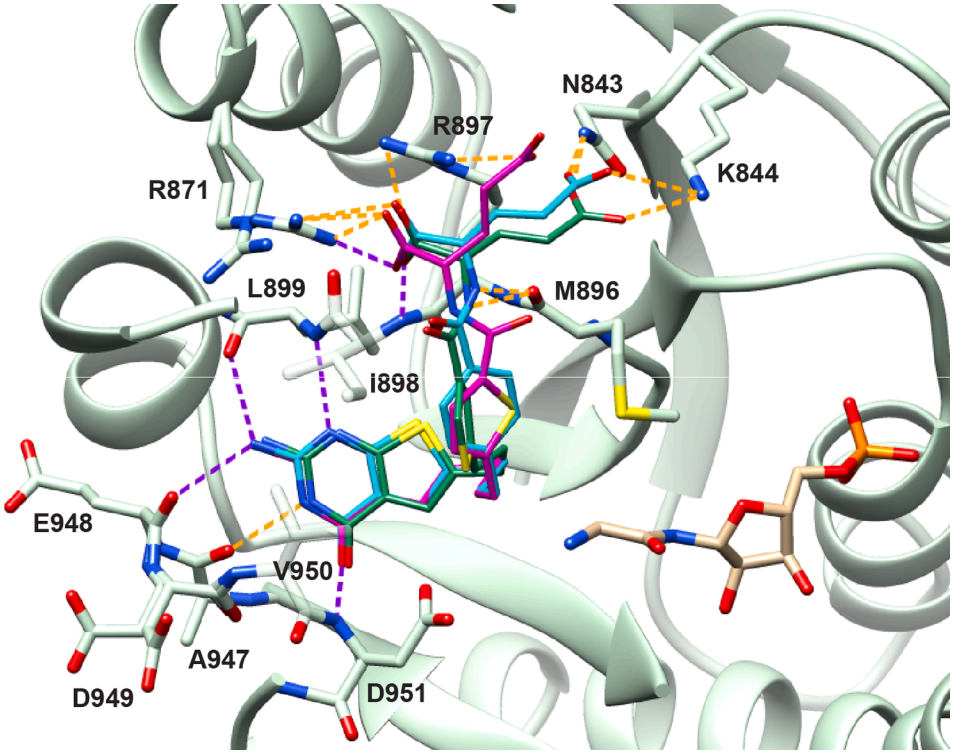


**Figure 4.** Molecular modeling studies of compounds **2, 3** and **7** with human GARFTase (PDB 4ZYW).[50,51] Superimposition of the docked poses of **2** (cyan, −15.02 kcal/mol), **3** (magenta, −14,82 kcal/mol) and **7** (green, −16.26 kcal/mol). The substrate GAR is shown in tan. Polar contacts are depicted in dashed lines, where purple lines show conserved interactions between the crystal structure complexes and the docked models. Contacts shown as orange dashes are unique to docked models. For comparison, ligand contacts for the crystallographic starting model, 4ZYW, are provided in the Supporting Information (**Figure S1**). Docking studies were performed using Maestro 12.3 (Schrödinger LLC).[53.]

with the backbone amide of Ile898. The γ-carboxylate of **2** and **7** are oriented similarly, forming polar interactions with Asn843 and Lys844, while the amide of the glutamyl tail hydrogen bonds with the backbone carbonyl of Met896. In contrast, the γ-carboxylate of **3** was only able to form polar contacts with Arg897.

We docked compounds **2** and **3**–**9** in the AICARFTase domain of the crystal structure of human ATIC (PDB 1P4R).[52] Compounds **3** and **4** show slightly lower docked scores than **2**; further modification of the aromatic side-chain afforded compounds **5**–**9,** which showed slightly better docked scores than the lead compound **2**. All the compounds **3**–**9** afforded better docked scores than PMX (Table 1). Docked poses for compound **2** and designed analogs **3** and **7**, as examples, are shown in Figure 5. The 2-$NH_2$ position of the bicyclic scaffold of the thieno[2,3-*d*] pyrimidine analogs forms hydrogen bonds with Asp546 and Asn489. The N3 hydrogen bonds with Asp546 and the 4-oxo moiety hydrogen bonds with the NH of Asn547 in all examples. Finally, the S7 of the bicyclic scaffold of all analogs forms an interaction with the side-chain of Ser450. The aromatic bridges of **2**, **3** and **7** show nonpolar contacts to Phe315. The L-glutamate moieties of **3** and **7** bind differently from the aryl L-glutamate moiety of **2.** The α-carboxylates of **2** and **3** form salt

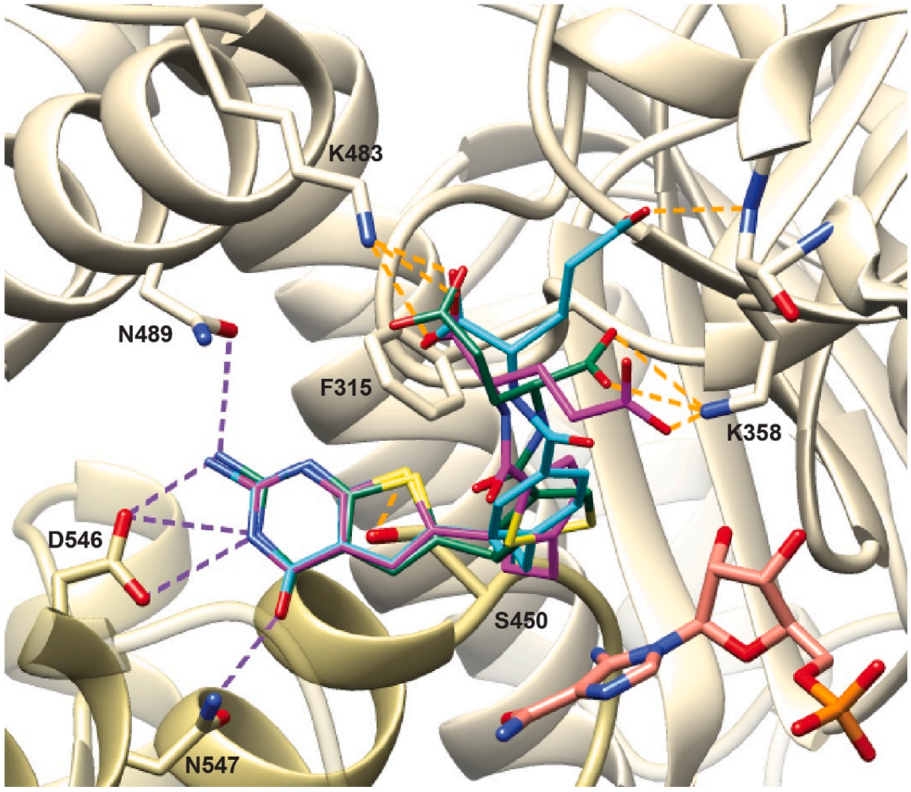


**Figure 5.** Molecular modeling studies with **2**, **3** and **7** in human AICARFTase (PDB: 1P4R).[52] Superimposition of the docked poses of **2** (cyan, −12.91 kcal/mol), **3** (magenta, −12.54 kcal/mol), and **7** (green, −13.08 kcal /mol). Polar contacts are depicted as dashed lines, where purple lines show conserved interactions between the crystal structure complexes and the docked models. Contacts shown as orange dashes are unique to the docked models. For comparison, ligand contacts for the crystallographic starting model, 1P4R, are provided in the Supporting Information (**Figure S1**). Docking studies were performed and visualized using Maestro 12.3 (Schrödinger LLC).[53.]

bridges with Lys483. However, the glutamyl tail of **7** is flipped relative to **3,** the γ-carboxylate of **7** forming a hydrogen bond with Lys483 instead. The γ-carboxylate of **2** hydrogen bonds with the backbone amide of Lys358. In comparison, the γ-carboxylate of **3** and α-carboxylate of **7**, respectively, make salt bridge interactions with the side-chain of Lys358.

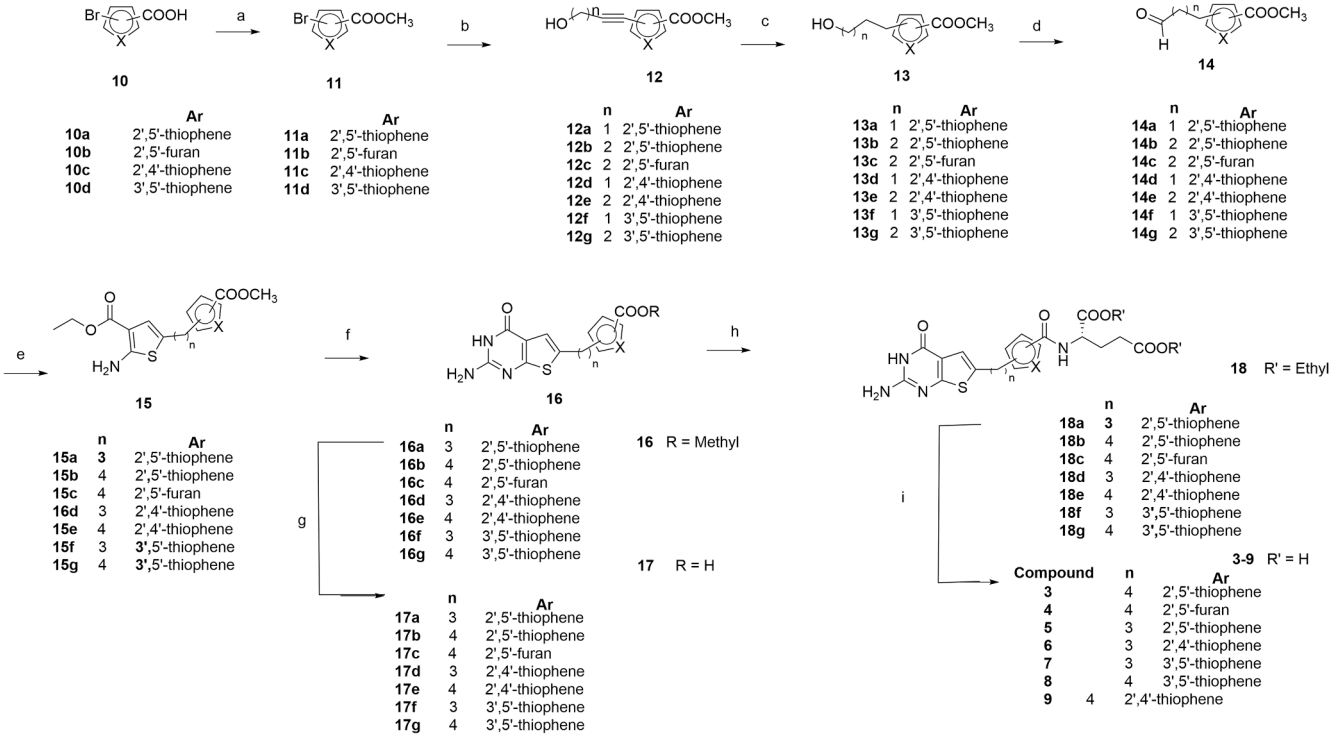


| 10 | Ar |
|---|---|
| 10a | 2',5'-thiophene |
| 10b | 2',5'-furan |
| 10c | 2',4'-thiophene |
| 10d | 3',5'-thiophene |

| 11 | Ar |
|---|---|
| 11a | 2',5'-thiophene |
| 11b | 2',5'-furan |
| 11c | 2',4'-thiophene |
| 11d | 3',5'-thiophene |

| 12 | n | Ar |
|---|---|---|
| 12a | 1 | 2',5'-thiophene |
| 12b | 2 | 2',5'-thiophene |
| 12c | 2 | 2',5'-furan |
| 12d | 1 | 2',4'-thiophene |
| 12e | 2 | 2',4'-thiophene |
| 12f | 1 | 3',5'-thiophene |
| 12g | 2 | 3',5'-thiophene |

| 13 | n | Ar |
|---|---|---|
| 13a | 1 | 2',5'-thiophene |
| 13b | 2 | 2',5'-thiophene |
| 13c | 2 | 2',5'-furan |
| 13d | 1 | 2',4'-thiophene |
| 13e | 2 | 2',4'-thiophene |
| 13f | 1 | 3',5'-thiophene |
| 13g | 2 | 3',5'-thiophene |

| 14 | n | Ar |
|---|---|---|
| 14a | 1 | 2',5'-thiophene |
| 14b | 2 | 2',5'-thiophene |
| 14c | 2 | 2',5'-furan |
| 14d | 1 | 2',4'-thiophene |
| 14e | 2 | 2',4'-thiophene |
| 14f | 1 | 3',5'-thiophene |
| 14g | 2 | 3',5'-thiophene |

| 15 | n | Ar |
|---|---|---|
| 15a | 3 | 2',5'-thiophene |
| 15b | 4 | 2',5'-thiophene |
| 15c | 4 | 2',5'-furan |
| 16d | 3 | 2',4'-thiophene |
| 15e | 4 | 2',4'-thiophene |
| 15f | 3 | 3',5'-thiophene |
| 15g | 4 | 3',5'-thiophene |

| 16 | n | Ar |
|---|---|---|
| 16a | 3 | 2',5'-thiophene |
| 16b | 4 | 2',5'-thiophene |
| 16c | 4 | 2',5'-furan |
| 16d | 3 | 2',4'-thiophene |
| 16e | 4 | 2',4'-thiophene |
| 16f | 3 | 3',5'-thiophene |
| 16g | 4 | 3',5'-thiophene |

| 17 | n | Ar |
|---|---|---|
| 17a | 3 | 2',5'-thiophene |
| 17b | 4 | 2',5'-thiophene |
| 17c | 4 | 2',5'-furan |
| 17d | 3 | 2',4'-thiophene |
| 17e | 4 | 2',4'-thiophene |
| 17f | 3 | 3',5'-thiophene |
| 17g | 4 | 3',5'-thiophene |

| 18 | n | Ar |
|---|---|---|
| 18a | 3 | 2',5'-thiophene |
| 18b | 4 | 2',5'-thiophene |
| 18c | 4 | 2',5'-furan |
| 18d | 3 | 2',4'-thiophene |
| 18e | 4 | 2',4'-thiophene |
| 18f | 3 | 3',5'-thiophene |
| 18g | 4 | 3',5'-thiophene |

| Compound | n | Ar |
|---|---|---|
| 3 | 4 | 2',5'-thiophene |
| 4 | 4 | 2',5'-furan |
| 5 | 3 | 2',5'-thiophene |
| 6 | 3 | 2',4'-thiophene |
| 7 | 3 | 3',5'-thiophene |
| 8 | 4 | 3',5'-thiophene |
| 9 | 4 | 2',4'-thiophene |

[a]**Reagents and conditions**: (a) LiOH, THF, dimethylsulfate, reflux, 3h, 77-96%; (b) $PdCl_2$,CuI, ACN, triethylaminetriphenylphosphine, 4-pentyn-1-ol or 5-hexyn-1-ol, 100 °C, μW, 70-80% (c) $H_2$ ,Pd/C, 55 psi, 79-96%; (d) Dess–Martin periodinane, $CH_2Cl_2$, 0°C to rt, 79-92%; (e) EtOH, $NEt_3$, Ethyl cyanoactetate,$S_8$ , 100°C, μW,40-71%; (f) $DMSO_2$, Choroformamidine hydrochloride,120 °C, 33-48% (g) 1N NaOH, rt,85-96%; (h) 4-Methylmorpholine, 2-chloro-4,6-dimethoxy-1,3,5-triazine, diethyl-*L*-glutamate hydrochloride, DMF,rt (i) 1N NaOH, rt, 32-40% over two steps.

**Scheme 1.**

Our first generation of 6-substituted thieno[2,3-*d*]pyrimidine analog **2**[40] with a 4 carbon bridge and side-chain benzene showed inhibition of human GARFTase and AICARFTase (Table 3). For the 2nd generation analogs of this series, we introduced modifications of the aromatic side-chain with various aryl replacements of the phenyl moiety, including positional 2′,5′-(compounds **3** and **5**), 2′,4′- (compounds **6** and **9**), and 3′,5′- (compounds **7** and **8**) thiophene isomers and a furan ring (compound **4**) (Figure 2**)**. Based on docking scores (Table 1), we hypothesize that most of these analogs would show superior GARFTase inhibition compared to compound **2**, while also retaining AICARFTase inhibition and directed tumor delivery via FRs. Our goal is to establish structure–activity relationships (SARs) for transport by FRs vis á vis RFC, and targeting of *de novo* purine nucleotide biosynthesis, including target duplicity at GARFTase and AICARFTase.

## 3. Chemistry

Target compounds **3**–**9** were synthesized, as shown in Scheme 1. The appropriate carboxylic acid **10** was esterified under basic conditions to afford the methyl ester **11**. A palladium-catalyzed cross-coupling of the bromo-thiophene ester **11** with the appropriate alcohol provided **12** (70–80% yield). Catalytic reduction of the triple bond of **12** gave the alcohol **13** (79–96% yield). Dess–Martin periodinane oxidation of **13** afforded the aldehyde **14** in 79–92% yield. Gewald reaction of **14** under microwave conditions provided the thiophene **15** in 40–71% yield. Cyclization of **15** with chloroformamidine hydrochloride in dimethyl sulfone afforded the thieno[2,3-*d*]pyrimidine ester **16** in 33–48% yield. Hydrolysis of the methyl ester of **16** followed by acid workup gave the corresponding acid **17** in 85–96% yield. With 2-Cl-4,6-dimethoxy-1,3,5-triazine and 4-methyl morpholine as the coupling reagents, acid **17** was coupled with diethyl-*L*-glutamate hydrochloride to afford compound **18**. Hydrolysis of **18** in 1 N NaOH, followed by acid workup, gave target compounds **3**–**9** in 32–40% yield over two steps.

## 4. Biological evaluation and discussion

### 4.1. Anti-proliferative effects of 6-substituted thieno[2,3-d]pyrimidine analogs in relation to mechanisms of folate transport

We compared the *in vitro* efficacy of compounds **3**–**9** to the parent 6-substituted thieno[2,3-*d*]pyrimidine compound **2** from our prior study.[40] As an initial screen for inhibitory potential, we tested growth inhibition of our novel analogs toward a unique panel of isogenic Chinese hamster ovary (CHO) sublines. The CHO cells were derived from the RFC-, FR- and PCFT-null MTXRIIOua$^{R}$2-4 CHO subline (R2)[54] and were engineered to individually express each of the major human folate transporters including FRα (RT16), FRβ (D4), RFC (PC43-10), or PCFT (R2/PCFT).[7,40,55,56] Thus, differences in anti-proliferative activities resulting from treatment with our inhibitors reflect specificities for transport. Initial screening of the CHO sublines used a fluorescence-based viability assay[7] to measure cell proliferation during continuous exposure to the compounds (up to 1000 nM) over 96 h.

Results obtained with the PC43-10 and R2/PCFT4 CHO cells were compared to those with R2 cells as controls. To confirm FR-mediated uptake for the RT16 and D4 sublines, we treated cells with 200 nM folic acid, completely blocking FR-uptake.[15,48] We compared our results for the thienopyrimidine compounds with those for the classical C1 inhibitors MTX and PMX that show little-to-no tumor selectivity as they are transported by RFC, PCFT and FRs.[31] Further, experiments were performed in RFC-, PCFT- and FR-expressing human tumor cells, including KB nasopharyngeal epidermoid carcinoma and NCI-IGROV1 EOC cells.

Widely disparate results were obtained for the 6-substituted thieno[2,3-*d*]pyrimidine compounds toward the CHO sublines, depending on the expressed transporter. None of thieno[2,3-*d*]pyrimidine analogs showed evidence of transport by human RFC, as reflected in a lack of effect on cell proliferation up to 1000 nM inhibitor in RFC-expressing PC43-10 cells (Table 2). Whereas most of the compounds showed no impact on cell proliferation for PCFT-expressing R2/PCFT4 cells, **6** (2′,4′-thiophene) and **7** (3′,5′-thiophene) displayed moderate inhibition of cell proliferation on par with that for the 6-substituted pyrrolo[2,3-*d*]pyrimidine compound **AGF23** (Figure 1) in our prior study.[55]

Cellular uptake by FRs was reflected in loss of cell proliferation for the RT16 (FRα) and D4 (FRβ) cell lines. For FRα-expressing RT16 cells, the $IC_{50}$s ranged from ~ 0.3–10 nM and were in the order of potency, **5** > **6** > **7** = **8** > **3** > **9** > **4** (Table 2). FRβ results were similar with the exception of compounds **4** and **5** which showed disparate sensitivities toward D4 CHO cells versus RT16 cells. Notably, most of the compounds showed increased potencies over those for compound **2**, as reflected in decreased $IC_{50}$ values. Importantly, R2 cells, which lack all folate transporters, were not inhibited by any of the 6-substituted thieno[2,3-*d*]pyrimidine analogs up to 1000 nM, indicating that these analogs all require transport into cells. For all the compounds and FR-targeted cells, inhibition of cell proliferation was completely reversed by 200 nM folic acid.

In KB tumor cells, compounds **3**–**9** displayed inhibition with $IC_{50}$s ranging from ~ 1 to 8 nM and like the FRα-expressing RT16 cells, inhibition was completely reversed by addition of excess folic acid. Although KB cells express all the major folate transporters, the complete reversal of drug effects by folic acid establishes the primary route of entry for the 6-substituted thieno[2,3-*d*]pyrimidine analogs to be via FRα rather than by RFC or PCFT.[15,48]

The *in vitro* inhibition experiments were extended to a FRα-expressing EOC cell model, NCI-IGROV1.[57] Potency was reduced in NCI-IGROV1 cells compared to KB cells (at least in part reflecting decreased FRα levels in NCI-IGROV1 cells[7]); inhibition was seen for most analogs in the order **3** > **7** ≫ **5** > **6** = **9** with $IC_{50}$s ranging from ~ 10 to ~ 100 nM. Surprisingly, compounds **4** and **8** showed no inhibition of cell proliferation up to 1000 nM. Again, all the active compounds showed complete reversal of inhibition when folic acid was added to parallel wells, suggesting that the major uptake mechanism in NCI-IGROV1 cells is via FRα endocytosis.

### 4.2. FR binding affinities of thieno[2,3-d]pyrimidine analogs

The results in the CHO and human tumor cell lines in Table 2 establish that the novel thienopyrimidine analogs **3**–**9** are selectively transported by FRs. While compounds **6** and **7** are also substrates for PCFT, in KB and NCI-IGROV1 tumor cells, uptake by FRα predominated, as reflected in inhibition of cell proliferation that was completely abolished in the presence of excess folic acid. As binding to FRs is requisite for internalization, we measured competition with [$^{3}$H]folic acid surface binding at 4 °C for select compounds (**3**–**5**) over a range of inhibitor concentrations (0–1 μM) with FRα and FRβ-expressing CHO cells[7] (Table 2). In this assay, relative inhibitor binding affinities were reflected in their abilities to compete with [$^{3}$H]folic acid for FR binding compared to non-radioactive folic acid (positive control) and MTX (negative control) (Figure 6). An additional control included compound **2**.[40] Bound [$^{3}$H]folic acid to FRs was quantified and normalized to total cell protein. Relative binding affinities to FRs were calculated as the inverse molar ratio of unlabeled ligand necessary to decrease FR-bound [$^{3}$H]folic acid by 50%, with folic acid assigned a relative value of 1 (Figure 6).

For both FRα- (RT16) and FRβ- (D4) expressing cells, compounds **3**–**5** showed binding affinities (89–150% and 60–112% of that for folic acid for FRα and FRβ, respectively), similar to those previously reported for compound **2**[40] (Figure 6). There were only modest differences in relative binding affinities between the FRα and FRβ isoforms and there was no direct correlation between relative FR binding affinities and anti-proliferative activities for compounds **2**–**5** (Table 2).

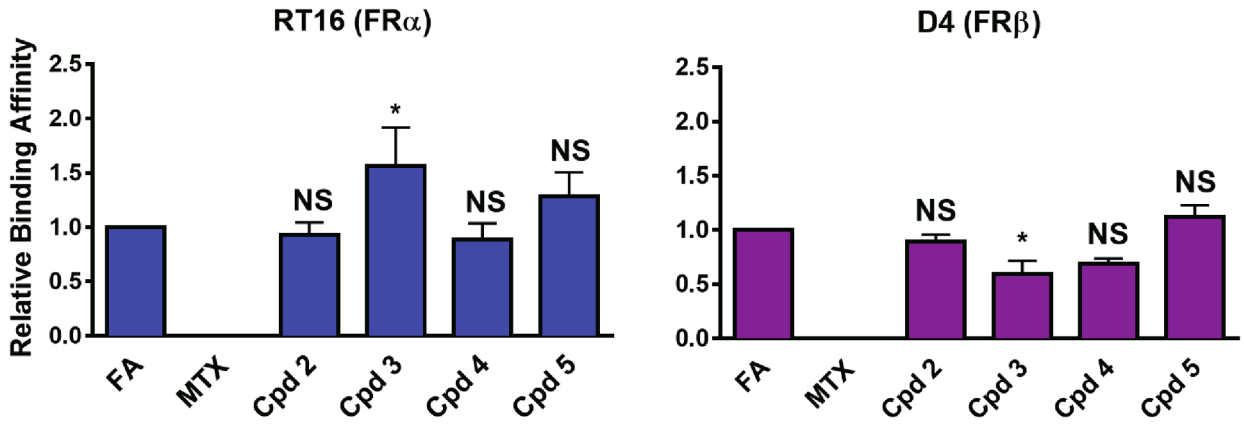


**Figure 6. FRα and FRβ binding affinities for compounds 2, 3, 4, and 5, compared to folic acid and MTX.** Results are shown for the relative binding affinities of the thieno[2,3-*d*]pyrimidine compounds **2**, **3**, **4** and **5** with FRα-expressing RT16 cells and FRβ-expressing D4 CHO cells. Relative binding affinities were determined over a range of inhibitor concentrations and were calculated as the inverse molar ratios of the unlabeled ligands required to inhibit [$^{3}$H]folic acid binding by 50%. By this definition, the relative affinity of folic acid is 1. Detailed experimental methods are provided in the Experimental Section. Abbreviations: FA, folic acid; NS, not significant. Data are mean values +/- standard deviations for 3–5 replicates. Statistical comparisons were with folic acid, as appropriate. *, $p < 0.05$. Results with compound **2** was previously published.[40.]

### *4.3. Identification of de novo purine biosynthesis as pathway of inhibition for 6-substituted thieno[2,3-d]pyrimidine analogs*

*De novo* purine biosynthesis involves 10 steps from phosphoribosyl pyrophosphate to IMP including two folate-dependent steps catalyzed by GARFTase (reaction 3: GAR → formyl GAR (fGAR)) and AICARFTase (reaction 9: ZMP → formyl AICAR (FAICAR)). FAICAR is metabolized to IMP by IMP synthase and subsequently to GMP and AMP (Figure 8**A**). To identify the targeted pathway for the 6-substituted thieno[2,3-*d*]pyrimidine analogs, we performed nucleoside protection experiments in

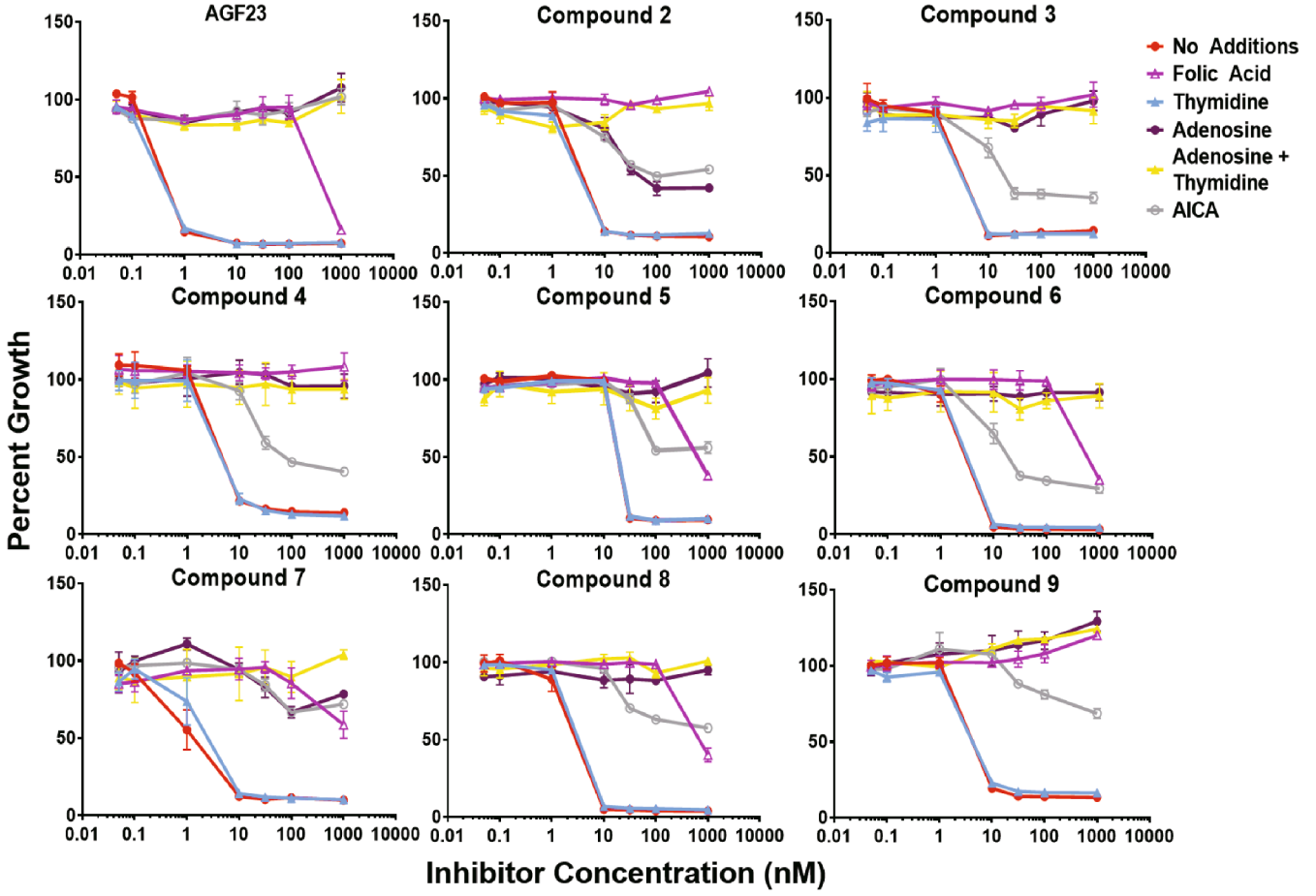


**Figure 7. Growth inhibition of KB human tumor cells by 6-substituted thieno[2,3-*d*] pyrimidine analogs 2–9 compared to AGF23 and and protective effects of excess folic acid, nucleosides, or AICA.** KB cells were plated (4000 cells/well) in 96 well plates with a range of drug concentrations, in the presence of folic acid (200 nM), adenosine (60 μM), thymidine (10 μM), or AICA (320 μM). Cell proliferation was assayed with a fluorescence-based assay.[7] Data are representative of at least triplicate experiments. Results are summarized in Table 2. The methods are described in the Experimental Section.

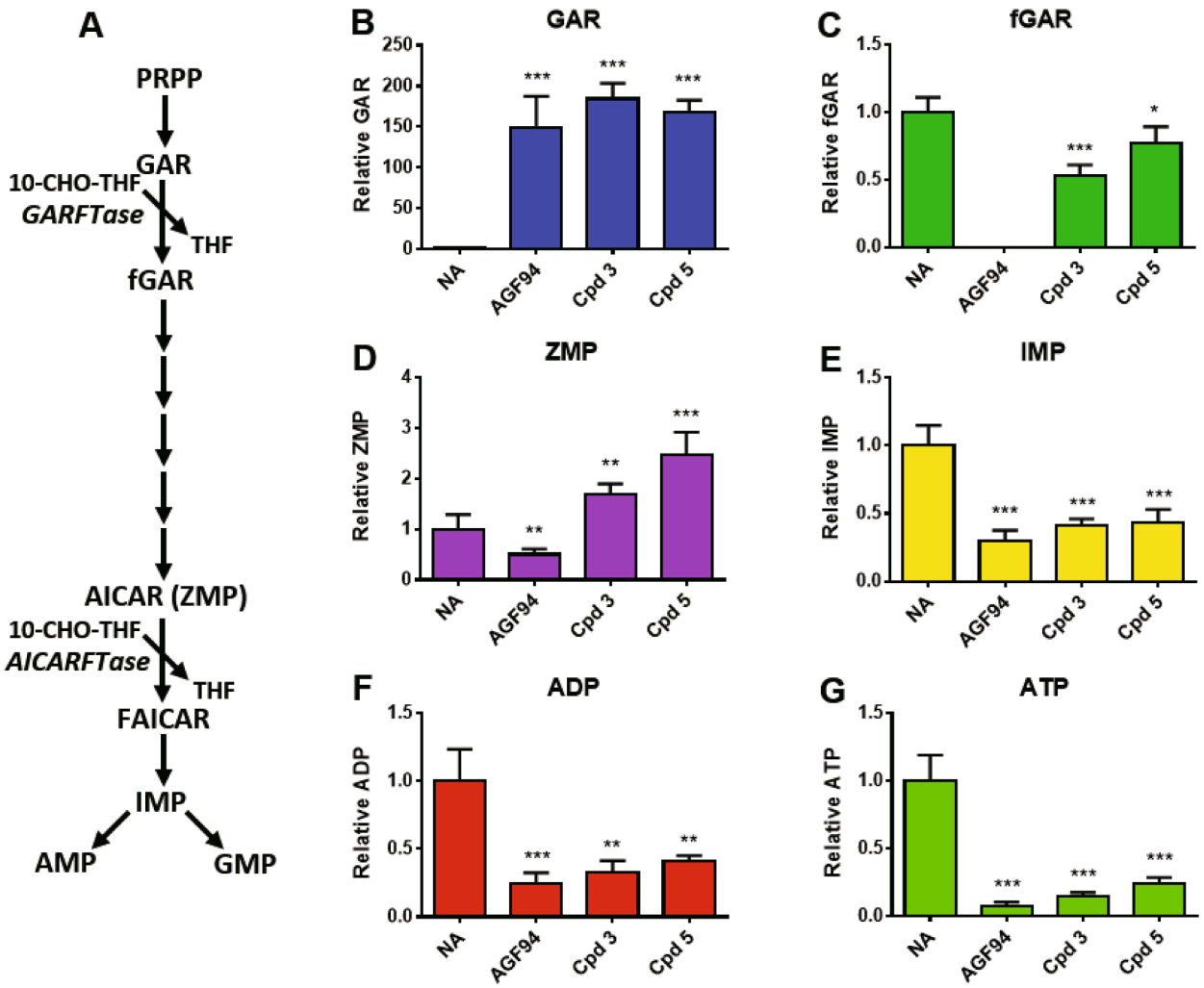


**Figure 8. Targeted metabolomics analysis in NCI-IGROV1 EOC cells to identify intracellular targets for 3 and 5.** A: *De novo* purine biosynthetic pathway showing the 10 reactions from PRPP to IMP including the 10-formyl tetrahydrofolate (10-CHO-THF)-dependent reactions catalyzed by GARFTase and AICARFTase. B-G: Relative GAR, ZMP, fGAR, IMP, ADP, and ATP levels compared to control cells (no additions, NA). Data are mean values +/- standard deviations for five technical replicates. #, $p < 0.10$; *, $p < 0.05$; **, $p < 0.01$; ***, $p < 0.001$; NS = not significant. Statistical comparisons were with vehicle-treated control samples. Detailed experimental methods are provided in the Experimental Section. Undefined abbreviations: THF, tetrahydrofolate.

KB human tumor cells. We compared results for compounds **3**–**9** to those for **AGF23** (Figure 1) (inhibits only GARFTase[7]) and compound **2** (Figure 2) (inhibits both GARFTase and AICARFTase[34,40]; Table 3). We initially tested exogenous adenosine (60 μM) and thymidine (10 μM) for their capacities to rescue KB cells from the inhibitory effects of active analogs as a measure of their inhibition of *de novo* purine nucleotide and thymidylate biosynthesis, respectively.[7] Whereas thymidine was completely ineffective in reversing drug effects, all compounds were completely protected by adenosine (Figure 7 and Table 2). This established purine nucleotide biosynthesis as the targeted pathway.

To begin to identify the targeted reaction in the purine biosynthetic pathway, we tested the protective effects of AICA (320 μM), which circumvents GARFTase by providing substrate for AICARFTase via its metabolism to ZMP.[34,40] While AICA completely protected cells from the inhibitory effects of **AGF23**, as expected for a GARFTase inhibitor with no significant inhibition of AICARFTase,[7] AICA provided variable protection for the other analogs (Figure 7). As previously reported,[40] AICA provided incomplete protection for compound **2**. This metabolic protection profile extended to the expanded cohort of thieno[2,3-*d*]pyrimidine compounds **3**–**9**. Thus, based on the results of the nucleoside/AICA protection experiments, compounds **3**–**9** likely inhibit *de novo* purine biosynthesis at AICARFTase, although inhibition by GARFTase cannot be excluded.

### 4.4. Identification of intracellular enzyme targets of 6-substituted thieno [2,3-*d*]pyrimidine analogs through targeted metabolomics

To directly assess the metabolic impact by our 6-substituted thieno [2,3-*d*]pyrimidine analogs and to further confirm inhibition of intracellular enzyme targets in *de novo* purine nucleotide biosynthesis suggested from our nucleoside protection experiments (Figure 7), we measured intracellular metabolites with targeted metabolomics. For these experiments, NCI-IGROV1 EOC cells were treated with compounds **3** and **5**, as prototypes of the thieno[2,3-*d*]pyrimidine series, and the results were compared to those for the established GARFTase inhibitor **AGF94**[36] (Figure 8).

NCI-IGROV1 cells were treated with 1 μM of the inhibitors for 48 h. The metabolites GAR, fGAR, ZMP, IMP, ATP, ADP and AMP were extracted and measured by LC-MS/MS.[4] For all inhibitors, we observed a substantial increase (150–200-fold) in the level of the GARFTase substrate GAR (Figure 8**B**). The level of the GARFTase product fGAR was decreased ~ 99% in the **AGF94**-treated cells, reflecting potent GARFTase inhibition as reported.[36,50] In contrast, fGAR levels were substantial and approached those in the control for cells treated with

compounds **3** (~50% of control) and **5** (~75% of control) (Figure 8**C**). This suggests incomplete inhibition of GARFTase by these compounds. The AICARFTase substrate ZMP (AICAR) was decreased (~50%) in NCI-IGROV1 cells treated with **AGF94**, as expected for a selective GARFTase inhibitor. However, for **3** and **5**, ZMP increased (2- and 3-fold, respectively), in support of a direct inhibition of AICARFTase by these compounds (Figure 8**D**).

We also investigated the effects of C1 inhibitors on assorted purine nucleotides including IMP, AMP, ADP and ATP. We observed a ~ 60% decrease in IMP, a 75–85% decrease in ATP and a 60–70% decrease in ADP with all the thieno[2,3-*d*]pyrimidine inhibitors (Figure 8**E, F, G**). Variations in AMP levels were modest or insignificant (not shown).

These results further establish the direct inhibition of *de novo* purine biosynthesis by compounds **3** and **5**. They also establish a pattern of inhibition for compounds **3** and **5** most consistent with direct targeting of both GARFTase and AICARFTase.

### 4.5. *In vitro confirmation of enzyme targets with isolated GARFTase and AICARFTase*

To further confirm the enzyme targets for the thieno[2,3-*d*]pyrimidine inhibitors identified from our nucleoside/AICA protection studies with compounds **3**–**9** (Figure 7) and metabolomics experiments with compounds **3** and **5** (Figure 8), we performed *in vitro* assays with purified GARFTase and ATIC (AICARFTase)[4] to calculate inhibition dissociation constants ($K_i$s) for compound inhibition (Table 3). Results were compared to those for the lead compound **2**. Compounds **3**–**9** inhibited both enzyme targets with micromolar $K_i$s, thus validating results of our *in vitro* cell-based assays. The $K_i$s for GARFTase spanned a ~ 70-fold range with potencies in rank order **8** > **7** > **3** > **2** > **6** = PMX > **5** > **4**. For AICARFTase, the $K_i$s for AICARFTase spanned a ~ 24-fold range with potencies in rank order **8** = PMX > **3** > **9** = **7** = **2** > **5** > **6** > **4**. Thus, for both GARFTase and AICARFTase, a 4 carbon bridge and 3′,5′-thieno ring (compound **8**) are preferred with ~ 20-fold and ~ 9-fold decreased $K_i$s over the previous lead compound **2**. Conversely, a 4 carbon bridge and furan ring (compound **4**) afforded the least potent inhibitor for both enzyme targets (Table 3). Thus, to an approximation, potencies for GARFTase and AICARFTase correlate with the distances between the thieno[2,3-*d*]pyrimidine scaffold and the L-glutamate (Table 1). Notably, MTX primarily inhibits DHFR[8] and is a comparatively modest inhibitor of GARFTase and AICARFTase.

While *in vitro* cell-free enzyme assays for compounds **2**–**9** establish target feasibility and relative potencies between analogs, these results only partially reflect those for the *in vitro* efficacy studies in tumor cells (Table 2) in that they do not encompass the contributions of membrane transport and conversion to polyglutamates that typically enhance affinities for target enzymes,[8,11] let alone the impact of multi-enzyme associations of purine enzymes (i.e., "purinosome") which are important to the efficient flux of pathway intermediates and synthesis of purine nucleotides.[58,59] Most importantly, the *in vitro* enzyme inhibition studies confirm dual inhibition of GARFTase and AICARFTase catalytic activities, further validating the results of the molecular modeling studies (Table 1), cell-based nucleoside/AICA protection and metabolomics experiments (Figures 7 and 8).

### 4.6. *X-Ray crystal structures of 6-substituted thieno[2,3-d]pyrimidine antifolates with human GARFTase*

To directly assess whether molecular variations in the 6-substituted thieno[2,3-*d*]pyrimidine analogs contributed to different binding modes of GARFTase, we determined the structures of select analogs (**3**, **4**, and **5**) with human GARFTase and β-GAR substrate and compared these to the GARFTase structure of compound **2**.[50] The thieno[2,3-*d*]pyrimidine scaffolds of all analogs make polar contacts with the backbone atoms of Leu899, Glu948, and Asp951 in GARFTase (**Figures S2-S4**). Compound **3** was the most potent inhibitor of the structures solved with GARFTase ($K_i$ = 1.36 μM) (Table 3). In addition to the peptide backbone contacts, the binding of the L-glutamyl tail of **3** is mediated by contacts with Lys844, Arg871, and Arg897. In contrast, compounds **2** ($K_i$ = 2.97 μM) and **5** ($K_i$ = 8.19 μM) do not make contacts in the bridge or L-glutamyl tail, which correlates with less potent inhibition against GARFTase compared to **3** (**Figure S4**). Compound **4** ($K_i$ = 10.72 μM) was one of the least potent molecules against GARFTase (Table 3). Similar to **3**, the glutamyl tail of **4** makes additional contacts with the side-chain of Arg871 and the backbone of Arg897. However, the γ-carboxylate of the L-glutamyl tail of **4** does not make direct contact with Lys844. This likely reflects the shorter distance between the scaffold the and L-glutamate in **4** compared to **3** (Table 1). Rather, the γ-carboxylate coordinates two additional water molecules with Asn843 and Lys844, suggesting that the positioning and direct interaction of the γ-carboxylate of the glutamyl tail are important for potency of this analog. Thus, the contacts with the enzyme were not shared amongst all these complexes; i.e., distinct contacts were predicted to confer varying inhibition potencies and are summarized in Figure 9**E.**

## 5. Conclusions

Multi-targeted agents offer significant advantages over single target agents for cancer and are especially attractive as a means of circumventing chemotherapy drug resistance. *De novo* purine nucleotide biosynthesis is a critical metabolic pathway in malignant cells[59] and inhibition of purine nucleotide biosynthesis has several advantages in that it kills tumors independent of wild-type/mutant p53 status,[60] shows tumor selectivity based on impaired purine salvage,[61] and results in suppression of mTOR signaling, a key tumor pro-survival pathway.[32,62]

In this report, we describe results of an investigation into the SAR for a novel rationally designed series of 6-substituted thieno[2,3-*d*]pyrimidine antifolates with aryl bridge modifications as inhibitors of *de novo* purine biosynthesis at GARFTase and AICARFTase. We previously reported a 6-substituted pyrrolo[2,3-*d*]pyrimidine compound (**AGF23**) with a benzoyl side-chain that inhibits GARFTase as its sole intracellular target and is transported by both FRs and PCFT over RFC.[7] Isosteric replacement of the pyrrole with a thieno ring in the bicyclic scaffold provides increased ring size and affords a hydrogen bond acceptor (S) in lieu of a hydrogen bond donor (NH). Combined with different bridge lengths (3- or 4- carbons), these modifications determine both the conformation and the distance between the scaffold and L-glutamate, thus impacting access to cellular targets critical to anti-tumor activity.

From proliferation assays in engineered CHO cells individually expressing RFC, PCFT or FRs, we showed that the anti-proliferative activities of the thieno[2,3-*d*]pyrimidine compounds were mediated principally through FRs. These findings were extended to KB human tumor cells and, for the majority of compounds, to NCI-IGROV1 human EOC cells, characterized by moderate levels of FRα similar to those found in primary EOCs.[15] In general, the newer thieno[2,3-*d*]pyrimidine inhibitors were more potent inhibitors toward FR-expressing cells than the previously described side-chain phenyl compound **2**.[40] Further, activity appeared to be enhanced for analogs with shorter bridge lengths (3- versus 4-carbons), although this association was not absolute. For a small subset of compounds (**6** and **7**), PCFT-transport activity was detected. Inhibitor uptake by PCFT is of potential interest, since for tumors such as EOC, FR expression is heterogeneous and changes with stage and grade, whereas PCFT expression is constitutive.[15] Thus, PCFT would afford an additional means of cytotoxic drug delivery for these compounds separate from FRs for tumors with lower FR levels.[15] Most importantly, the complete lack of detectable RFC targeting for this series would preclude significant toxicities toward normal tissues, a remarkable advantage over MTX and PMX.[8,11, 12]

As predicted by the molecular modeling studies, the thieno[2,3-*d*]pyrimidine C1 inhibitors with modifications to the bridge region (3- or 4- carbons) and a side-chain aromatic ring (thiophene, furan) were suggested by nucleoside/AICAR protection studies to be direct inhibitors

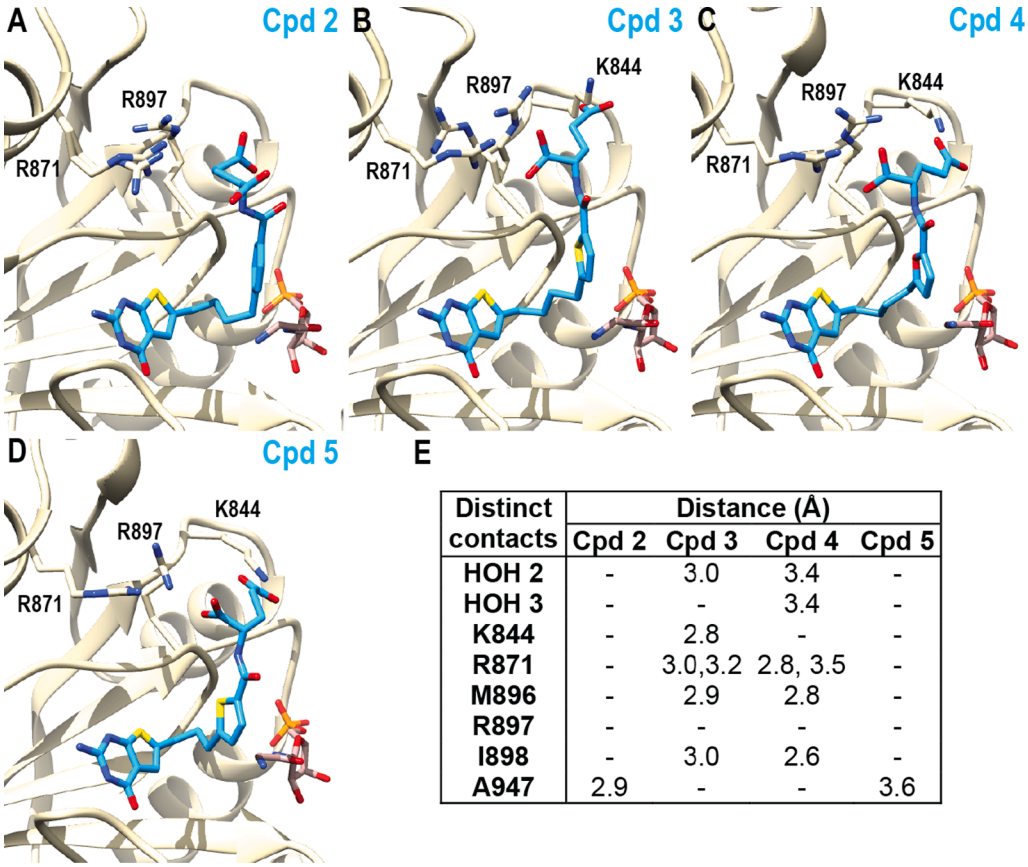


| Distinct contacts | Distance (Å) | | | |
|---|---|---|---|---|
| | Cpd 2 | Cpd 3 | Cpd 4 | Cpd 5 |
| HOH 2 | - | 3.0 | 3.4 | - |
| HOH 3 | - | - | 3.4 | - |
| K844 | - | 2.8 | - | - |
| R871 | - | 3.0,3.2 | 2.8, 3.5 | - |
| M896 | - | 2.9 | 2.8 | - |
| R897 | - | - | - | - |
| I898 | - | 3.0 | 2.6 | - |
| A947 | 2.9 | - | - | 3.6 |

**Figure 9. Structural analyses of 6-substituted pyrollo- and thieno[2,3-*d*]pyrimidine analogs in GARFTase-β-GAR-antifolate ternary complexes.** (A) Crystal structure of compound **2**[40] (cyan) bound in the 10-CHO-THF binding pocket of GARFTase with the natural substrate β-GAR (brown) and interacting residues shown as sticks. Also shown are the structures of (B) **3**, (C) **4**, and (D) **5**, and (E) a table summarizing distinct analog contacts (i.e., not seen universally in all crystal structures). See the main text for description of shared contacts. Data processing and refinement statistics (**Table S1**), as well as detailed interactions and maps for the complexes (**Figures S2-S4**), are included in the Supporting Information. The structure for **2** was previously reported.[50]

of both GARFTase and AICARFTase. This was confirmed by targeted metabolomics profiling with significantly depleted ATP pools and IMP pools, accompanied by substantial increases in both GAR and AICAR. Our *in vitro* enzyme inhibition studies confirmed dual targeting of GARFTase and AICARFTase, although enzyme inhibition in cells would likely be enhanced by compound metabolism to polyglutamates.[8]

Through structural studies with GARFTase and β-GAR, we determined that the peptide backbone and L-glutamyl tail contacts in GARFTase were critical for more potent inhibition, along with positioning and interaction of the γ-carboxylate of the L-glutamyl tail. This observation was exemplified by the difference in GARFTase inhibition for compounds **3** and **4**. Although we identified compound **8** as the most potent dual GARFTase and AICARFTase inhibitor of this series, *in vitro* drug efficacy did not always reflect inhibitor potency measured by direct enzyme assay. Indeed, compound **8** inhibited proliferation of KB tumor cells but was inert toward NCI-IGROV1 EOC cells, in contrast to compounds such as **3** and **5** that were less potent GARFTase inhibitors. This further establishes the importance of cellular pharmacodynamics (e.g., transport, polyglutamylation) to anti-tumor drug efficacies for this this series of analogs.

Collectively, our results document a novel first-in-class series of thieno[2,3-*d*]pyrimidine inhibitors with FR selectivity and inhibition of a critical metabolic pathway to malignant cells, resulting in potent anti-tumor activity. This series affords an exciting new platform for development of selective multi-targeted anti-tumor agents.

## 6. Experimental section

### 6.1. Experimental

Melting points were determined on a Mel-Temp II melting point apparatus with FLUKE 51 K/J electronic thermometer and were uncorrected. Nuclear magnetic resonance spectra for proton ($^1$H) were recorded on a Bruker 500 MHz spectrometer or Bruker 400 MHz spectrometer. The chemical shift values were expressed in ppm (parts per million) relative to tetramethylsilane as an internal standard; s = singlet, d = double, t = triplet, q = quartet, m = multiplet, br = broad singlet. The relative integrals of peak areas agreed with those expected for the assigned structures. Thin-layer chromatography (TLC) was performed on WHATMAN UV254 silica gel plates with a fluorescent indicator, and the spots were visualized under 254 and/or 365 nm illumination. Proportions of solvents used for TLC were by volume. Column chromatography was performed on 230–400 mesh silica gel purchased from ThermoFisher Scientific. All evaporations were carried out under reduced pressure using a rotary evaporator. Analytical samples were dried under reduced pressure (0.2 mm Hg) in an Chem-Dry drying apparatus over $P_2O_5$ at 50–80 °C. Elemental analysis was performed by Altlantic Microlabs, Norcross, GA. Element compositions are within ± 0.4% of calculated values. Fractional moles of water or organic solvents frequently found in some analytical samples could not be prevented despite 24–48 h of drying under reduced pressure and were confirmed where possible by their presence in the $^1$H NMR spectra. All solvents and chemicals were purchased from Strem Chemicals Inc., Sigma-Aldrich Chemical Co. or Fisher Scientific. All the chemicals and the solvents were used as received unless stated otherwise. In some cases, solvents were degassed using freeze–thaw cycle.

### 6.2. Synthesis of compounds

#### 6.2.1. General procedure for the synthesis of compounds 11.

To a 250 mL round-bottom flask, fitted with a magnetic stir bar, the carboxylic acid **10** (2.07 g, 10 mmol) was dissolved in THF; lithium hydroxide was added (0.43 g, 21 mmol) and the mixture was stirred for 30 min at room temperature. Dimethyl sulfate (1,152 g, 12 mmol) was

added and kept at reflux for 2 h. Silica gel (4.0 g) was added, and the solvent was evaporated under reduced pressure. The resulting plug was loaded on a silica gel column and eluted with 5% ethyl acetate in hexane. Fractions that showed the desired spot (TLC) were collected, and the solvent evaporated under reduced pressure to afford methyl esters **11** as a yellow or colorless liquid or solid.

**Methyl 5-bromothiophene-2-carboxylate (11a)**. The general method described for the preparation of target compounds from 5-bromothiophene-2-carboxylic acid, **10a** (2.07 g, 10 mmol) was used to prepare **11a** as a colorless liquid (1.8 g, 81.44%); TLC $R_f$ 0.78 (Hexane/Ethyl Acetate = 1:1). $^1$H NMR (400 MHz, Chloroform-*d*): $\delta$ 3.90 (s, 3H, $CH_3$), 7.10 (d, $J$ = 3.9 Hz, 1H, CH, Ar), 7.58 (d, $J$ = 3.9 Hz, 1H, CH, Ar).

**Methyl 5-bromofuran-2-carboxylate (11b).** The general method described for the preparation of target compounds from 5-bromofuran 2-carboxylic acid, **10b** (1.89 g, 10 mmol) was used to prepare **11b** as a white solid (1.93 g, 95%); TLC $R_f$ 0.55 (Hexane/Ethyl Acetate = 3:1). $^1$H NMR (DMSO-$d_6$): $\delta$ 3.80 (s, 3H), 6.84–6.85 (d, 1H, $J$ = 3.6 Hz), 7.35–7.36 (d, 1H, $J$ = 3.6 Hz).

**Methyl 4-bromothiophene-2-carboxylate (11c)**. The general method described for the preparation of target compounds from 4-bromothiophene-2-carboxylic acid, **10c** (2.07 g, 10 mmol) was used to prepare **10c** as a colorless liquid (1.9 g, 85%); TLC $R_f$ 0.78 (Hexane/Ethyl Acetate = 1:1). $^1$H NMR (400 MHz, Chloroform-*d*): $\delta$ 3.88 (s, 3H, $CH_3$), 7.441(d, 1H, $J$ = 1.4 Hz, CH, Ar), 7.70 (d, 1H, $J$ = 1.4 Hz, CH, Ar).

**Methyl 5-bromothiophene-3-carboxylate (11d)**. The general method described for the preparation of target compounds from 5-bromothiophene-3-carboxylic acid, **10d** (2.07 g, 10 mmol) was used to prepare **11d** as a light yellow liquid (1.72 g, 77.84%); TLC $R_f$ 0.78 (Hexane/Ethyl Acetate = 1:1). $^1$H NMR (400 MHz, Chloroform-*d*): $\delta$ 3.88 (s, 3H, $CH_3$), 7.50 (d, $J$ = 1.3 Hz ,1H, CH, Ar), 8.01 (d, $J$ = 1.3 Hz ,1H, CH, Ar).

*6.2.2. General procedure for the synthesis of compounds 12.*

To a 20 mL microwave vial with a stir bar was added the appropriate bromothiophene-carboxylic acid methyl ester (1.10 g, 5 mmol) in anhydrous acetonitrile (10 mL), palladium chloride (35.5 mg, 0.82 mmol), triphenylphosphine (65 mg, 0.2 mmol), copper iodide (152 mg, 0.8 mmol), trimethylamine (5.50 g, 50 mmol), and 4-pentyn-1-ol or 5-hexyn-1-ol (7.5 mmol). The reaction mixture was heated to 100 °C in the microwave for 1 h. The reaction was cooled and silica gel (10 g) was added; the solvent was evaporated under reduced pressure to afford a plug which was loaded on to a silica gel column and eluted with hexane followed by 20% ethyl acetate in hexane. Fractions that showed the desired spot (TLC) were pooled and evaporated to afford **12** as a light-yellow liquid.

**Methyl 5-(5-hydroxypent-1-yn-1-yl)thiophene-2-carboxylate (12a)**. The general method described for the preparation of target compounds from **11a** (2.20 g, 20 mmol) was used to prepare **12a** as a light-yellow liquid (1.86 g, 80.96%); TLC $R_f$ 0.36 (Hexane/Ethyl Acetate = 1:1). $^1$H NMR (400 MHz, Chloroform-*d*): $\delta$ 1.90 (m, 2H, $CH_2$), 2.61(t, $J$ = 7.0 Hz ,2H, $CH_2$), 3.84 (t, 2H, $CH_2$), 3.90 (s, 3H, $CH_3$), 7.08 (d, $J$ = 3.9 ,1H, CH, Ar), 7.65 (d, $J$ = 3.9 Hz ,1H, CH, Ar).

**Methyl 5-(6-hydroxyhex-1-yn-1-yl)thiophene-2-carboxylate (12b)**. The general method described for the preparation of target compounds from **11b** (2.20 g, 20 mmol) was used to give **12b** as a light-yellow liquid (1.76 g, 79.26%); TLC $R_f$ 0.37 (Hexane/Ethyl Acetate = 1:1). $^1$H NMR (400 MHz, Chloroform-*d*): $\delta$ 1.74 (m, 4H, $CH_2$), 2.53 (t, 2H, $CH_2$), 3.74 (t, $J$ = 11.8 Hz, 2H, $CH_2$), 3.90 (s, 3H, $CH_3$), 7.08 (d, $J$ = 3.9 Hz ,1H, CH, Ar), 7.65 (d, $J$ = 3.8 Hz, 1H, CH, Ar).

**Methyl 5-(6-hydroxyhex-1-yn-1-yl)furan-2-carboxylate (12c).** The general method described for the preparation of target compounds from **11c** (2.20 g, 20 mmol) was used to prepare **12c** as a light-yellow liquid (1.86 g, 85%); TLC $R_f$ 0.28 (hexane/ Ethyl Acetate 1:1). $^1$H NMR (400 MHz, DMSO-$d_6$): $\delta$ 1.51–1.58 (m, 4H), 3.39–3.43 (m, 2H), 3.79 (s, 3H), 4.42–4.45 (t, 1H, $J$ = 5.2 Hz, OH exch), 6.83–6.84 (d, 1H, $J$ = 3.6 Hz), 7.30–7.31 (d, 1H, $J$ = 3.6 Hz).

**Methyl 4-(5-hydroxypent-1-yn-1-yl)thiophene-2-carboxylate (12d).** The general method described for the preparation of target compounds from **11d** (2.20 g, 10 mmol) was used to prepare **12d** as a light-yellow liquid (1.44 g, 70.27%); TLC $R_f$ 0.35 (Hexane/Ethyl Acetate = 1:1). $^1$H NMR (400 MHz, Chloroform-*d*): $\delta$ 1.91–1.83 (m, 2H, $CH_2$), 2.54 (t, 2H, $CH_2$), 3.83 (t, 2H, $CH_2$), 3.91 (s, 3H, $CH_3$), 7.53 (d, $J$ = 1.4 Hz 1H, CH, Ar), 7.75 (d, 1H, $J$ = 1.4 Hz, CH, Ar).

**Methyl 4-(6-hydroxyhex-1-yn-1-yl)thiophene-2-carboxylate (12e).** The general method described for the preparation of target compounds from **11e** (2.20 g, 10 mmol) was used to prepare **12e** as a light-yellow liquid (1.63 g, 70.90%); TLC $R_f$ 0.36 (Hexane/Ethyl Acetate = 1:1). $^1$H NMR (400 MHz, Chloroform-*d*): $\delta$ 1.80–1.65 (m, 2H, $CH_2$), 2.54 (t, 2H, $CH_2$), 3.83(t, $J$ = 6.0 Hz ,2H, $CH_2$), 3.91(s, 3H, $CH_3$), 7.53(d, $J$ = 1.4 Hz, 1H, CH), 7.75(d, $J$ = 1.4 Hz ,1H, CH, Ar).

**Methyl 5-(5-hydroxypent-1-yn-1-yl)thiophene-3-carboxylate (12f).** The general method described for the preparation of target compounds from **11f** (2.20 g, 10 mmol) was used to prepare **12f** as a light-yellow liquid (1.58 g, 72%); TLC $R_f$ 0.36 (Hexane/Ethyl Acetate = 1:1). $^1$H NMR (400 MHz, Chloroform-*d*): $\delta$ 1.89 (m, 2H, $CH_2$), 2.59 (t, $J$ = 7.0 Hz, 2H, $CH_2$), 3.83 (d, $J$ = 3.8 Hz, 2H, $CH_2$), 3.88 (s, 3H,$CH_3$), 7.51 (d, $J$ = 1.2 Hz, 1H, Ar),7.94 (d, $J$ = 1.3 Hz, 1H, Ar).

**Methyl 5-(6-hydroxyhex-1-yn-1-yl)thiophene-3-carboxylate (12g)**. The general method described for the preparation of target compounds from **11g** (2.20 g, 10 mmol) was used to prepare **12g** as a light-yellow liquid (1.70 g, 71.94%); TLC $R_f$ 0.37(Hexane/Ethyl Acetate = 1:1). $^1$H NMR (400 MHz, Chloroform-*d*): $\delta$ 1.73 (m, 4H, $CH_2$), 2.08 (t, 2H, $CH_2$), 2.50 (t, 2H, $CH_2$), 3.89 (s, 3H, $CH_3$), 7.51(d, $J$ = 1.3 Hz, 1H, CH, Ar), 7.94(d, $J$ = 1.3 Hz ,1H, CH, Ar).

*6.2.3. General procedure for the synthesis of compounds 13:*

To a Parr hydrogenation flask was added **12** (8.02 mmol), 10% palladium on activated carbon (400 mg), and methanol (50 mL). Hydrogenation was carried out at 55 psi of $H_2$ for 4 h. The reaction mixture was filtered through celite, washed with methanol (100 mL), and concentrated under reduced pressure to give **13** as a light-yellow liquid.

**Methyl 5-(5-hydroxypentyl)thiophene-2-carboxylate (13a).** Using the general procedure, **13a** was obtained from **12a** as a light-yellow liquid (1.63 g, 90.5%); TLC $R_f$ 0.36 (Hexane/Ethyl Acetate = 1:1).[1] $^1$H NMR (400 MHz, Chloroform-*d*): $\delta$ 1.45(m, 2H, $CH_2$), 1.73(m, 4H, $2CH_2$), 2.86(m, $J$ = 7.6 Hz ,2H, $CH_2$), 3.66 (t, $J$ = 6.5 Hz 2H, $CH_2$), 3.87(s, 3H, $CH_3$), 6.80 (d, $J$ = 3.7 Hz, 1H, CH, Ar), 7.64 (d, $J$ = 3.7 Hz ,1H, CH, Ar).

**Methyl 5-(6-hydroxyhexyl)thiophene-2-carboxylate (13b).** Using the general procedure, **13b** was obtained from **12b** as a light-yellow liquid (1.58 g, 81%); TLC $R_f$ 0.37 (Hexane/ Ethyl Acetate = 1:1). $^1$H NMR (400 MHz, Chloroform-*d*) : $\delta$ 1.350–1.445 (m, 4H, $2CH_2$), 1.60(m, 2H, $2CH_2$), 1.72(m, 2H, $2CH_2$), 2.86(m, 2H, $2CH_2$), 3.67 (t, $J$ = 6.6 Hz, 2H, $CH_2$), 3.89(s, 3H, $CH_3$) $\delta$ 6.80 (d, $J$ = 3.7 Hz , 1H, CH, Ar) $\delta$ 7.66 (d, $J$ = 3.7 Hz ,1H, CH, Ar).

**Methyl 5-(6-hydroxyhexyl)furan-2-carboxylate (13c).** Using the general procedure, **13c** was obtained as a light-yellow liquid (2.09 g, 90%); TLC $R_f$ 0.35 (hexane/Ethyl Acetate = 1:1). $^1$H NMR (DMSO-$d_6$): $\delta$ 1.27–1.30 (m, 4H), 1.36–1.42 (m, 2H), 1.55–1.62 (m, 2H), 2.64–2.68 (t, 2H), 3.33–3.38 (m, 2H), 3.76 (s,3H), 4.31–4.34 (t, 1H, $J$ = 5.2 Hz, OH), 6.33–6.41 (d, 1H, $J$ = 3.6 Hz), 7.19–7.20 (d, 1H, $J$ = 3.6 Hz).

**Methyl 4-(5-hydroxypentyl)thiophene-2-carboxylate (13d)**. Using the general procedure, **13d** was obtained from compound **12d** as a light-yellow liquid (1.46 g, 79%); TLC $R_f$ 0.35 (Hexane/Ethyl Acetate = 1:1).[1] $^1$H NMR (400 MHz, Chloroform-*d*): $\delta$ 1.350–1.445(m, 2H, $CH_2$), 1.65(qd, $J$ = 15.0, 7.1 Hz, $2CH_2$), 2.64(m, 2H, $CH_2$), 3.67(t, $J$ = 6.5 Hz ,2H, $CH_2$), 3.89(s, 3H, $CH_3$), 6.80(d, 1.5 Hz, 1H, CH, Ar), 7.65 (d, 1.5 Hz ,1H, CH, Ar).

**Methyl 4-(5-hydroxypentyl)thiophene-2-carboxylate (13e)**. Using the general procedure, **13e** was obtained from **12e** as a light-yellow liquid (1.69 g, 92.33%); TLC $R_f$ 0.36 (Hexane/ Ethyl Acetate = 1:1). $^1$H NMR (400 MHz, Chloroform-*d*): $\delta$ 1.350–1.445(m,4H, $2CH_2$),

1.65(m, 4H, $2CH_2$), 2.64(m, $J = 7.6$ Hz,2H, $CH_2$), 3.67(t, $J = 6.5$ Hz ,2H, $CH_2$), 3.89(s, 3H, $CH_3$), 7.17(d, 1.4 Hz, 1H, CH, Ar),7.65 (d, 1.4 Hz, 1H, CH, Ar).

**Methyl 5-(5-hydroxypentyl)thiophene-3-carboxylate (13f).** Using the general procedure, **13f** was obtained from **12f** as a light-yellow liquid (1.58 g, 86%); TLC $R_f$ 0.36 (Hexane/Ethyl Acetate = 1:1). $^1$H NMR (400 MHz, Chloroform-*d*): $\delta$ 1.47(m, 2H, $CH_2$), 1.78 – 1.69 (m, 4H, $2CH_2$), 2.84(m, 2H, $CH_2$), 3.67 (t, 2H, $CH_2$), 3.87 (s, 3H, $CH_3$), 7.22 (d, $J = 1.2$ Hz, 1H, CH, Ar), 7.91 (d, $J = 1.2$ Hz, 1H, CH, Ar).

**Methyl 5-(6-hydroxyhexyl)thiophene-3-carboxylate (13g).** Using the general procedure, **13g** was obtained from **12g** as a light-yellow liquid (1.76 g, 96%); TLC $R_f$ 0.37 (Hexane / Ethyl Acetate = 1:1). $^1$H NMR (400 MHz, Chloroform-*d*): $\delta$ 1.42 (m, 4H, $CH_2$), 1.60 (m, 2H, $CH_2$), 1.72 (m, 2H, $CH_2$), 2.82 (m, 2H, $CH_2$), 3.67 (t, 2H, $CH_2$), 3.87 (s, 3H, $CH_3$), 7.21(d, $J = 1.2$ Hz ,1H, CH, Ar), 7.91 (d, $J = 1.2$ Hz ,1H, CH, Ar).

*6.2.4. General procedures for the synthesis of 14.*

To a solution of compound **13** (1.5 g, 6.4 mmol) in anhydrous dichloromethane (10 mL) in a round bottom flask cooled in an ice bath was added a stirred solution of Dess-Martin periodinane (DMP) (2.96 g, 6.9 mmol) in dichloromethane (8 mL) at 0 ℃, and the mixture was allowed to warm from 0 C to rt. After 3 h, when the TLC showed the disappearance of **13**, 10 mL of 1 N sodium hydroxide solution was added to deactivate the remaining DMP, followed by extraction with ethyl acetate (3 × 30 mL). Fractions that showed the desired product (TLC) **14** were pooled and evaporated to dryness; this afforded **14** as a yellow liquid.

**Methyl 5-(5-oxopentyl)thiophene-2-carboxylate (14a).** Using the general procedure, **14a** was obtained as a light-yellow liquid (1.53 g, 83%); TLC $R_f$ 0.70 (Hexane/Ethyl Acetate = 1:1). $^1$H NMR (400 MHz, Chloroform-*d*): $\delta$ 1.78–1.70 (m, 2H, $CH_2$), 2.50 (td, $J = 6.7$, 2H, $CH_2$), 2.88 (t, $J = 7.1$ Hz, $CH_2$), (d, $J = 1.0$ Hz, 2H), 3.88 (s, 3H, $CH_3$), 6.81 (d, $J = 3.7$ Hz 1H, CH), 7.65 (d, $J = 3.7$ Hz ,H, CH), 9.79 (t, $J = 1.5$ Hz, 1H, CHO).

**Methyl 5-(6-oxohexyl)thiophene-2-carboxylate (14b).** Using the general procedure, **14b** was obtained as a light-yellow liquid (1.81 g, 91%); TLC $R_f$ 0.68 (Hexane/Ethyl Acetate = 1:1). $^1$H NMR (400 MHz, Chloroform-*d*): $\delta$ 1.27–1.32 (m, 2H, $CH_2$), 1.49–1.53 (t, 2H, $CH_2$), 1.59–1.65 (t, $J = 7.1$ Hz, $CH_2$), 2.39–2.43 (t, 2H, $CH_2$), 3.77 (s, 3H, $CH_3$), 6.94 (d, $J = 3.7$ Hz, 1H, CH, Ar), 7.63(d, $J = 3.7$ Hz ,H, CH, Ar), 9.63(t, $J = 1.5$ Hz, 1H, CHO).

**Methyl 5-(6-oxohexyl)furan-2-carboxylate (14c).** Using the general procedure, **14c** was obtained as a light-yellow liquid (1.99 g, 95%); TLC $R_f$ 0.72 (hexane/Ethyl Acetate = 1:1). $^1$H NMR (400 MHz, DMSO-$d_6$) $\delta$ 1.24 (m, 2H), 1.60 (m, 4H), 2.43 (t, 2H), 2.68 (t, 2H), 3.68 (s, 3H, $CH_3$), 6.34–6.35 (d, 1H, $J = 3.6$ Hz), 7.20–7.21 (d, 1H, $J = 3.6$ Hz), 9.63–9.65 (t, 1 CHO).

**Methyl 4-(5-oxopentyl)thiophene-2-carboxylate (14d).** Using the general procedure, **14d** was obtained as a light-yellow liquid (1.76 g, 88%); TLC $R_f$ 0.67 (Hexane/Ethyl Acetate = 1:1). $^1$H NMR (400 MHz, DMSO-$d_6$): $\delta$ 1.54 (m, 4H, $2CH_2$), 2.46 (t, $J = 7.0$, 1.4 Hz, 2H,$CH_2$), 2.60 (t, $J = 7.1$ Hz 2H, $CH_2$), 3.80 (s, 3H, $CH_3$), 7.58 (d, $J = 1.5$ Hz 1H, CH, Ar), 7.68 (d, $J = 1.5$ Hz H, CH, Ar), 9.66 (t, $J = 1.5$ Hz 1H, CHO).

**Methyl 4-(5-oxopentyl)thiophene-2-carboxylate (14e**). Using the general procedure, **14e** was obtained as a light-yellow liquid (1.74 g, 87%); TLC $R_f$ 0.68 (Hexane/Ethyl Acetate = 1:1). $^1$H NMR (400 MHz, Chloroform-*d*): $\delta$ 1.54 (m, 4H, $2CH_2$), 1.72–1.60 (m, 4H, $2CH_2$), 2.60 (m, 2H, $CH_2$), 3.80 (s, 3H, $CH_3$), 7.58 (d, $J = 1.5$ Hz, 1H, CH, Ar), 7.68(d, $J = 1.5$ Hz, 1H, CH, Ar), 9.66 (t, $J = 1.7$ Hz ,1H, CHO).

**Methyl 5-(5-oxopentyl)thiophene-3-carboxylate (14f).** Using the general procedure, **14f** was obtained as a light-yellow liquid (1.82 g, 92%); TLC $R_f$ 0.69 (Hexane/Ethyl Acetate = 1:1). $^1$H NMR (400 MHz, Chloroform-*d*): $\delta$ 1.74(m, 4H, $2CH_2$), 2.50(m, 2H, $CH_2$), 2.85 (m, 2H, $CH_2$), 3.87(s, 3H, $CH_3$), 7.22(d, $J = 1.4$ Hz ,1H, CH, Ar), 7.92(d, H, CH, Ar), 9.79 (t, $J = 1.6$ Hz ,1H, CHO).

**Methyl 5-(6-oxohexyl)thiophene-3-carboxylate (14g**). Using the general procedure, **14g** was obtained as a light-yellow liquid (1.42 g, 71%); TLC $R_f$ 0.71 (Hexane/Ethyl Acetate = 1:1). $^1$H NMR (400 MHz, Chloroform-*d*): $\delta$ 1.42 (m, 2H, $CH_2$), 1.71 (m, 4H, $2CH_2$), 2.47(m, 2H, $CH_2$), 2.83 (m, 2H, $CH_2$), 3.86 (s, 3H, $CH_3$), 7.21 (d, $J = 1.3$ Hz 1H, CH), 7.91(d, $J = 1.3$ Hz, H, CH), 9.79 (t, $J = 1.7$ Hz ,1H, CHO).

*6.2.5. General procedures for the synthesis of 15.*

To a 20 mL microwave vial was added a solution of aldehyde **14** (6.18 mmol) with a mixture of sulfur (300 mg, 9.3 mmol), ethyl cyanoacetate (700 mg, 6.18 mmol), ethanol (15 mL) and triethylamine (68 mg, 0.62 mmol); the vial was sealed and subjected to microwave irradiation at 80 °C for 30 min. Unreacted sulfur was removed by filtration, and the filtrate was concentrated under reduced pressure to afford an orange liquid. The residue was loaded on a silica gel column and eluted with 10% ethyl acetate in hexane. Fractions were pooled and evaporated to afford the desired products.

**Methyl 5-(3-(5-amino-4-(ethoxycarbonyl)thiophen-2-yl)propyl) thiophene-2-carboxylate (15a).** Using the general procedure, **15a** was obtained from **14a** (1.49 g, 6.18 mmol) as a yellow liquid (1.58 g, 70%); TLC $R_f$ 0.73 (Hexane/Ethyl Acetate = 1:1). $^1$H NMR (400 MHz, Chloroform-*d*): $\delta$1.43 (t, 3H, $CH_3$), 1.61 (m, 2H, $CH_2$), 2.81 (m, 2H, $CH_2$), 3.18 (m, 2H, $CH_2$), 4.27–4.37 (m, 5H, $CH_2$ and $CH_3$), 5.83 (s, 2H, $NH_2$-exchange), 6.68 (d, 1H, CH, Ar), 6.81–6.82 (d, $J = 3.7$ Hz, 1H, CH, Ar), 7.65–7.66 (d, $J = 3.7$ Hz, H, CH, Ar).

**Methyl 5-(4-(5-amino-4-(ethoxycarbonyl)thiophen-2-yl)butyl) thiophene-2-carboxylate (15b).** Using the general procedure, **15b** was obtained from **14b** (1.40 g, 6.18 mmol) as a yellow liquid (1.55 g, 71%); TLC $R_f$ 0.74 (Hexane/Ethyl Acetate = 1:1). $^1$H NMR (400 MHz, DMSO-$d_6$): $\delta$ 1.20–1.24 (t, 3H, $CH_3$), 1.49–1.56 (m, 2H, $CH_2$), 1.60–1.67 (m, 2H, $CH_2$), 2.52–2.56 (m, 2H, $CH_2$), 2.83–2.86 (t, 2H, $CH_2$), 3.77 (s, 3H, $CH_3$), 4.10–4.15 (q, 2H, $CH_2$), 6.49(s, 1H, CH, Ar), 6.94–6.95(s, 1H, CH, Ar), 7.10 (s, 2H, $NH_2$-exchange), 7.65–7.66 (d, 1H, CH, Ar).

**Methyl 5-(4- [5-amino-4-(ethoxycarbonyl)thiophen-2-yl] butyl} furan-2-carboxylate (15c).** Using the general procedure, **15c** was obtained from **14c** (1.58 g, 6.18 mmol) as a yellow liquid (0.78 g, 41%); TLC $R_f$ 0.34 (hexane/Ethyl Acetate = 3:1). $^1$H NMR (DMSO-$d_6$) 1.20–1.24 (t, 3H, $J = 6.8$ Hz, $OCH_2CH_3$), 1.49–1.63 (m, 4H), 2.57–2.60 (t, 2H, $J = 7.2$ Hz), 2.68–2.70 (t, 2H, $J = 7.2$ Hz), 3.76 (s, 3H, $OCH_3$), 4.09–4.15 (q, 2H, $J = 6.8$ Hz, $OCH_2CH_3$), 6.33–6.34 (d, 1H, $J = 3.2$ Hz), 6.49 (s, 1H), 7.01 (s, 2H, 2-$NH_2$ exch), 7.19–7.20 (d, 1H, $J = 3.2$ Hz).

**Methyl 4-(3-(5-amino-4-(ethoxycarbonyl)thiophen-2-yl)propyl) thiophene-2-carboxylate (15d).** Using the general procedure, **15d** was obtained from **14d** (1.58 g, 6.18 mmol) as a yellow liquid (1.30 g, 69%); TLC $R_f$ 0.75 (Hexane/Ethyl Acetate = 1:1). $^1$H NMR (400 MHz, Chloroform-*d*): $\delta$ 1.36 (t,3H, $CH_3$) $\delta$ 1.93 (m, 2H, $CH_2$), 2.63 (t, $J = 7.0$ Hz, 2H, $CH_2$), 2.68 (m, 2H, $CH_2$), 4.31 – 4.25 (m, 2H, $CH_2$), 5.83 (s, 2H, $NH_2$-exchange), 6.68 (d, 1H, CH), 6.81–6.82 (d, $J = 1.5$ Hz ,1H,CH, Ar), 7.65–7.66 (d, $J = 1.5$ Hz ,1H,CH, Ar).

**Methyl 4-(4-(5-amino-4-(ethoxycarbonyl)thiophen-2-yl)butyl) thiophene-2-carboxylate (15e).** Using the general procedure, **15e** was obtained from **14e** (1.40 g, 6.18 mmol) as a yellow liquid (1.18 g, 55.12%); TLC $R_f$ 0.73 (Hexane/Ethyl Acetate = 1:1). $^1$H NMR (500 MHz, Chloroform-*d*): $\delta$ 1.28 (t, $J = 7.2$ Hz, 3H, $CH_3$), 1.67 (m, 4H, $2CH_2$), 2.6–2.8 (m, 4H, $2CH_2$), 3.89 (s, 3H, $CH_3$), 4.14 (q, $J = 7.2$ Hz, 2H, $CH_2$), 5.81 (s, 2H, $NH_2$-exchange), 6.63(s,1H, CH, Ar), 7.17 (d, $J = 1.4$ Hz, 1H, Ar), 7.64 (d, $J = 1.6$ Hz, 1H, Ar).

**Methyl 5-(3-(5-amino-4-(ethoxycarbonyl)thiophen-2-yl)propyl) thiophene-3-carboxylate (15f).** Using the general procedure, **15f** was obtained from **14f** (1.58 g, 6.18 mmol) as a yellow liquid (1.33 g, 61%); TLC $R_f$ 0.74 (Hexane/Ethyl Acetate = 1:1). $^1$H NMR (400 MHz, Chloroform-*d*): $\delta$1.36 (td, $J = 7.1$, 3.0 Hz, 3H, $CH_3$), 2.04–1.93 (m, 2H, $CH_2$), 2.67(t, $J = 7.0$ Hz ,2H, $CH_2$), 2.86 (t, $J = 7.5$ Hz, 2H, $CH_2$), 3.87 (s, 3H, $CH_3$), 4.29 (m, 2H, $CH_2$), 5.832 (s, 2H, $NH_2$-exchange), 6.68 (d, 1H, CH, Ar), 7.23 (d, $J = 1.4$ Hz 1H, CH, Ar), 7.93 (d, $J = 1.4$ Hz 1H, CH, Ar).

**Ethyl 2-amino-5-(4-(4-(methoxycarbonyl)thiophen-2-yl)butyl)**

**thiophene-3-carboxylate (15g).** Using the general procedure, **15g** was obtained from **14g** (1.40 g, 6.18 mmol) as a yellow liquid (0.84 g, 40%); TLC $R_f$ 0.75 (Hexane/Ethyl Acetate = 1:1). $^1$H NMR (400 MHz, Chloroform-*d*) $\delta$ 1.35 (m, 3H, $CH_3$), 1.67 (m, 2H, $CH_2$), 1.75 (m, 2H, $CH_2$), 2.63 (m, 2H, $CH_2$), 2.83 (t, $J = 7.3$ Hz, 2H, $CH_2$), 3.87 (s, 3H, $CH_3$), 4.30 (dt, 2H, $CH_2$), 5.80 (s, 2H, $NH_2$-exchange), 6.65 (s, 1H, CH, Ar), 7.21 (d, $J = 1.4$ Hz, 1H, Ar), 7.91 (d, $J = 1.4$ Hz, 1H, Ar).

*6.2.6. General procedures for the synthesis of 16.*

A mixture of the appropriate thiophene **15** (1equiv) and chloroformamidine hydrochloride (4 equiv) in $DMSO_2$ was heated at 140 ℃ for 4 h. The mixture was cooled to room temperature, 20 mL water was added, and ammonium hydroxide was used to neutralize the suspension. The brown solid, obtained by filtration, was washed with water and dried over $P_2O_5$ vacuum. The solids were either used directly in the next reaction or dissolved in ethanol, followed by the addition of silica gel (depending on the amount of material obtained). If the amount of the material was 400 mg or greater, it was dissolved in ethanol and silica was added; a dry silica plug was obtained after evaporation of the solvent under reduced pressure. The plug was loaded on a silica gel column and eluted with 10% methanol in chloroform. The fractions containing the desired product (TLC) were pooled and evaporated to afford the desired compounds. If the solids obtained after washing or drying was<400 mg, it was used directly in the next reaction without column purification (crude yield will be reported).

**Methyl 5-(3-(2-amino-4-oxo-3,4-dihydrothieno [2,3-*d*] pyrimidin-6-yl)propyl)thiophene-2-carboxylate (16a).** The general method described for the preparation of target compounds from compound **15a** (0.8 g, 2.2 mmol) was used to prepare **16a** (0.4 g, crude yield 52%) as a brown solid; TLC $R_f$ 0.51 (Chloroform/Methanol = 5:1); mp > 300 °C. $^1$H NMR (DMSO-$d_6$): $\delta$ 2.66–2.72 (m, 2H, $CH_2$), 2.79–2.82 (m, 2H, $CH_2$), 3.81 (s, 3H), 6.46 (s, 2H, 2-$NH_2$ exch), 7.20, 7.21 (d,1H), 7.62, 7.63 (d, 1H), 7.7 (s, 1H), 10.83 (s, 1H, 3-NH exch). This compound was used directly for the next reaction without further purification.

**Methyl 5-(4-(2-amino-4-oxo-3,4-dihydrothieno [2,3-*d*] pyrimidin-6-yl)butyl)thiophene-2-carboxylate (16b)**. The general method described for the preparation of target compounds from compound **15b** (1.20 g, 3.27 mmol) was used to prepare **16b** (0.57 g, 48%) as a brown solid; TLC $R_f$ 0.50 (Chloroform/Methanol = 5:1). mp > 300 °C $^1$H NMR (500 MHz, DMSO-$d_6$); : $\delta$ 1.72–1.60 (m, 4H, $2CH_2$), 2.74 (t, $J = 6.8$ Hz, 2H), 2.89 (t, $J = 7.1$ Hz, 2H), 3.79 (s, 3H, $CH_3$), 6.47 (s, 2H, $NH_2$), 6.83 (s, 1H, CH, Ar), 6.96 (d, 1H, CH, Ar), 7.62 (d, $J = 3.7$ Hz,1H, CH, Ar), 10.84 (s, 1H, NH). This compound was used directly for the next reaction without further purification.

**Methyl 5- [4-(2-amino-4-oxo-3,4-dihydrothieno [2,3-*d*] pyrimidin-6-yl)butyl] furan-2- carboxylate(16c).** The general method described for the preparation of target compounds was used to prepare **16c** (1.49 g, 88%) as a yellow solid; mp 172.9–173.4 °C; TLC $R_f$ 0.3 (MeOH/$CHCl_3$ = 1:6). $^1$H NMR (DMSO-$d_6$): $\delta$ 1.61–1.63 (m, 4H), 2.68–2.73 (m, 4H), 3.76 (s, 3H), 6.33–6.34 (d, 1H, $J = 3.6$ Hz), 6.45 (s, 2H, 2-NH2 exch), 6.79 (s, 1H), 7.19–7.20 (d, 1H, $J = 3.6$ Hz), 10.82 (s, 1H, 3-NH exch).

**Methyl 4-(3-(2-amino-4-oxo-3,4-dihydrothieno [2,3-*d*] pyrimidin-6-yl)propyl)thiophene-2-carboxylate (16d).** The general method described for the preparation of target compounds from compound **15d** (1.20 g, 3.40 mmol) was used to prepare **16d** (0.4 g, 33%) as a brown solid; TLC $R_f$ 0.51 (Chloroform/Methanol = 5:1). mp > 300 °C; $^1$H NMR (500 MHz, DMSO-$d_6$): $\delta$ 1.91(m, 2H, $CH_2$), 2.65(t, $J = 7.6$ Hz ,2H, $CH_2$), 2.71 (t, $J = 7.2$ Hz ,2H, $CH_2$), 3.81(s, 3H, $CH_3$), 6.47(s, 2H, $NH_2$), 6.83 (d, $J = 1.0$ Hz, 1H, Ar), 7.62 (d, 1H, CH), 7.71 (d, $J = 1.6$ Hz, 1H, CH, Ar), 10.84 (s, 1H, NH).

**Methyl 4-(4-(2-amino-4-oxo-3,4-dihydrothieno [2,3-*d*] pyrimidin-6-yl)butyl)thiophene-2-carboxylate (16e).** The general method described for the preparation of target compounds from compound **15e** (1.20 g, 3.27 mmol) was used to prepare **16e** (0.43 g, 34%) as a brown solid, TLC $R_f$ 0.51 (Chloroform/Methanol = 5:1). mp > 300 °C, $^1$H NMR (400 MHz, DMSO-$d_6$): $\delta$ 1.60 (s, 4H, $2CH_2$), 2.63 (t, $J = 7.1$ Hz, 2H, $CH_2$), 2.72 (t, $J = 6.8$ Hz, 2H, $CH_2$), 3.80 (s, 3H, $CH_3$), 6.47 (s, 2H, $NH_2$), 6.80 (s, 1H, Ar), 7.58 (d, $J = 1.5$ Hz, 1H, Ar), 7.67 (d, $J = 1.6$ Hz, 1H, Ar), 10.84 (s, 1H, NH).

**Methyl 5-(3-(2-amino-4-oxo-3,4-dihydrothieno [2,3-*d*] pyrimidin-6-yl)propyl)thiophene-3-carboxylate (16f).** The general method described for the preparation of target compounds from compound **15f** (1.20 g, 3.40 mmol) was used to prepare **16f** (0.355 g, crude 30%) as a brown solid. The compound was used immediately for the next reaction without any further purification.

**Methyl 5-(4-(2-amino-4-oxo-3,4-dihydrothieno [2,3-*d*] pyrimidin-6-yl)butyl)thiophene-3-carboxylate (16g).** The general method described for the preparation of target compounds from compound **15g** (1.20 g, 3.27 mmol) was used to prepare **16g** (0.354 g, crude 28%) as a brown solid. The compound was used immediately for the next reaction without any further purification.

*6.2.7. General procedure for the synthesis of compounds 17.*

To a solution of **16** in ethanol (10–50 mL) was added aq 1 N NaOH; the reaction mixture was stirred at room temperature for 12 h. The ethanol was evaporated under reduced pressure, and the residue was dissolved in water (5–10 mL). The solution was carefully acidified to pH 3 with the dropwise addition of 1 N HCl. The resulting suspension was left at 0 ℃ for an hour, and then the residue was collected by filtration, washed with water (5 mL), and dried over $P_2O_5$/vacuum at 50 ℃ to afford the free acids **17**. Compound **17** was used immediately for the next reaction without any further purification.

**5-(3-(2-amino-4-oxo-3,4-dihydrothieno [2,3-*d*] pyrimidin-6-yl) propyl)thiophene-2-carboxylic acid (17a**). The general method described for the preparation of target compounds from compound **16a** was used to prepare **17a** (0.142 g, 94%) as a brown solid; TLC $R_f$ 0.43 (MeOH/$CHCl_3$, 1:6 + 1 drop of HOAc); mp > 300 °C. $^1$H NMR (500 MHz, DMSO-$d_6$): $\delta$ 1.95 (, $J = 7.5$ Hz, 2H, $CH_2$), 2.76 (t, $J = 7.4$ Hz, 2H), 2.87 (t, $J = 6.8$ Hz, 2H, $CH_2$), 6.83 (s, 1H, CH, Ar), 6.47 (s, 2H, $NH_2$), 6.96 (d, $J = 3.6$ Hz, 1H, Ar), 7.67 (d, $J = 3.6$ Hz, 1H, Ar), 11.06 (s, 1H, NH). This compound was used directly for the next reaction without further purification.

**5-(4-(2-amino-4-oxo-3,4-dihydrothieno [2,3-*d*] pyrimidin-6-yl) butyl)thiophene-2-carboxylic acid (17b).** The general method described for the preparation of target compounds from compound **16b** (0.50 g, 1.38 mmol) was used to prepare **17b** (0.43 g, 89%) as a light brown solid. mp > 300 °C; TLC $R_f$ 0.43 (MeOH/$CHCl_3$, 1:6 + 1 drop of HOAc).[1] $^1$H NMR (500 MHz, DMSO-$d_6$): $\delta$ 1.59 (m, 4H, $2CH_2$), 2.74 (t, $J =$ 7.2 Hz, 2H, $CH_2$), 2.89 (d, $J = 7.2$ Hz, 2H, $CH_2$), 6.50 (s, 2H, $NH_2$), 6.93 (d, $J = 3.7$ Hz, 1H, Ar), 7.56 (d, $J = 3.7$ Hz, 1H, Ar), 10.88 (s, 1H, NH).

**5-(4-(2-amino-4-oxo-3,4-dihydrothieno [2,3-*d*] pyrimidin-6-yl) butyl] furan-2-carboxylic acid (17c).** The general method described for the preparation of target compounds from compound **16c** (0,16 g, 0.481 mmol) was used to prepare **17c** (0.13 g, 87%) as a light brown solid, mp > 300 °C; TLC $R_f$ 0.40 (MeOH/$CHCl_3$ = 1:6 + 1 drop of gl. HOAc); $^1$H NMR (DMSO-$d_6$) $\delta$ 1.62–1.63 (m, 4H), 2.67–2.74 (m, 4H), 6.29–6.30 (d, 1H, $J = 3.2$ Hz), 6.30 (s, 2H, 2-NH2 exch), 6.79 (s, 1H), 7.09–7.10 (d, 1H, $J = 3.2$ Hz), 10.83 (s, 1H, COOH exch), 12.78 (s, 1H, 3-NH exch).

**4-(3-(2-amino-4-oxo-3,4-dihydrothieno [2,3-*d*] pyrimidin-6-yl) propyl)thiophene-2-carboxylic acid (17d).** The general method described for the preparation of target compounds from compound **16d** (0.40 g, 1.10 mmol) was used to prepare **17d** (0.335 g, 92%) as a light brown solid; mp > 300 °C. $^1$H NMR (500 MHz, DMSO-$d_6$): $\delta$1.92 (t, 2H, $CH_2$), 2.64 (t, 2H, $CH_2$), 2.72 (t, 2H, $CH_2$), 6.48(s, 2H, $NH_2$), 6.82 (s, 1H, Ar), 7.61 (d, $J = 1.6$ Hz ,1H, Ar), 7.70 (d, $J = 1.6$ Hz, 1H, Ar), 10.83 (s, 1H, NH).

**4-(4-(2-amino-4-oxo-3,4-dihydrothieno [2,3-*d*] pyrimidin-6-yl) butyl)thiophene-2-carboxylic acid (17e).** The general method described for the preparation of target compounds from compound **16e** (0.40 g, 1.10 mmol) was used to prepare **17e** (0.37 g, 96%) as a light

brown solid; mp > 300 °C. $^1$H NMR (500 MHz, DMSO-$d_6$): δ1.59 (s, 4H, 2$CH_2$), 2.61 (t, $J$ = 7.0 Hz, 2H), 2.72 (t, $J$ = 6.6 Hz, 2H), 6.46 (s, 2H, $NH_2$), 6.80 (s, 1H, CH, Ar), 7.50 (s, 1H, CH, Ar), 7.58 (d, $J$ = 1.2 Hz, 1H, Ar), 10.84 (s, 1H, NH).

**5-(3-(2-amino-4-oxo-3,4-dihydrothieno [2,3-*d*] pyrimidin-6-yl) propyl)thiophene-3-carboxylic acid (17f).** The general method described for the preparation of target compounds from compound **16f** (0.40 g, 1.14 mmol) was used to prepare **17f** (0.363 g, 94%) as a light brown solid; mp > 300 °C. $^1$H NMR (400 MHz, DMSO-$d_6$): δ 1.94 (m, $J$ = 7.6 Hz, 2H, $CH_2$), 2.80 (m, 4H, 2$CH_2$), 6.70(s, 2H, $NH_2$), 6.85 (s, 1H, CH, Ar), 7.17 (s, 1H, CH, Ar), 8.06 (s, 1H, CH, Ar), 11.05 (s,1H, NH).

**5-(4-(2-amino-4-oxo-3,4-dihydrothieno [2,3-*d*] pyrimidin-6-yl) butyl)thiophene-3-carboxylic acid (17 g).** The general method described for the preparation of target compounds from compound **16 g** (0.46 g, 1.27 mmol) was used to prepare **17g** (0.375 g, 85%) as a light brown solid; mp > 300 °C. $^1$H NMR (500 MHz, DMSO-$d_6$): δ1.65 (m, 4H, 2$CH_2$), 2.74 (t, $J$ = 6.7 Hz, 3H), 2.83 (t, $J$ = 6.9 Hz, 2H), 6.48 (s, 2H, $NH_2$), 6.81 (s, 1H, Ar), 7.15 (s, 1H, CH, Ar), 8.04 (d, 1H, CH, Ar),10.86 (s, 1H, NH).

*6.2.8. General procedure for the synthesis of compound 18.*

To a solution of **17** (0.1 mmol) in anhydrous DMF (5–10 mL) was added *N*-methylmorpholine (0.12 mmol) and 2-chloro-4,6- dimethoxy-1,3,5-triazine (0.12 mmol). The resulting mixture was stirred at room temperature for 2 h, after which, *N*-methylmorpholine (0.12 mmol) and diethyl-L-glutamate hydrochloride (0.1 mmol) or dimethyl-L-glutamate hydrochloride were added to the mixture dropwise. The reaction mixture was stirred for an additional 3 h at room temperature, silica gel was added to this solution, and the suspension evaporated under reduced pressure. The plug obtained was loaded on a silica gel column and eluted with 2% methanol in chloroform. The fractions containing the desired product were pooled and evaporated to afford the products **18.** In cases where compounds were semi-solids and difficult to purify, the intermediates were used directly in the next reaction without further modification.

**Diethyl (5-(3-(2-amino-4-oxo-3,4-dihydrothieno [2,3-*d*] pyrimidin-6-yl)propyl)thiophene-2-carbonyl)-L-glutamate (18a).** The general method described for the preparation of target compounds from compound **17a** (0.13 g, 0.38 mmol) was used to prepare **18a** (0.155 g, 78%) as a yellow semi-solid. TLC $R_f$ 0.31 (MeOH/$CHCl_3$, 1:6); $^1$H NMR (DMSO-$d_6$): δ 1.13–1.19 (t, 6H), 1.95–2.23 (m, 2H Gluβ-$CH_2$), 2.40–2.44 (t, 2H, Gluγ-$CH_2$), 2.65–2.72 (m, 2H), 3.02–3.05 (m, 2H), 4.01–4.13(m, 4H), 4.41 (m, 1H, Gluα-CH), 6.48 (s, 2H, 2-NH2 exch), 6.86, 6.88 (d, 1H), 7.38,7.40 (d, 1H), 7.78, 7.79(d, 1H), 8. 63, 8.71 (d, 1H, CONH exch), 10.89 (s, 1H, 3-NH exch).

**Diethyl (5-(4-(2-amino-4-oxo-3,4-dihydrothieno [2,3-*d*] pyrimidin-6-yl)butyl)thiophene-2-carbonyl)-L-glutamate (18b).** The general method described for the preparation of target compounds from compound **17b** (0.34 g, 0.97 mmol) was used to prepare **18b** (0.388 g, 75%) as a yellow solid; mp 155.7–156.6 °C; TLC $R_f$ 0.33 (MeOH/$CHCl_3$, 1:6). $^1$H NMR (DMSO-$d_6$): δ1.413–1.19 (t, 6H), 1.64 (m, 4H), 1.93–2.13 (m, 2H Gluβ-$CH_2$), 2.38–2.42 (t, 2H, Gluγ-$CH_2$), 2.71–2.74 (t, 2H), 2.81–2.84 (t, 2H),4.01–4.13 (m, 4H), 4.33–4.39 (m, 1H, Gluα-CH), 6.44 (s, 2H, 2-$NH_2$ exch), 6.79(s, 1H), 6.87, 6.88 (d, 1H), 7.66, 7.67 (d, 1H), 8.59, 8.61 (d, 1H, CONH exch), 10.81 (s, 1H,3-NH exch). This compound was used directly for the next reaction without further purification.

**Diethyl *N*-({5- [4-(2-amino-4-oxo-3,4-dihydrothieno [2,3-*d*] pyrimidin-6-yl) butyl] furan-2- yl}carbonyl)-L-glutamate (18c).** The general method described for the preparation of target compounds from compound **17c** (0.15 g, 0.33 mmol) was used to prepare **18c** (0.102 g, 62%) as a light yellow semi-solid. mp 185.4–186.7 °C; TLC $R_f$ 0.33 (MeOH/$CHCl_3$ = 1:6).[1] $^1$H NMR (DMSO-$d_6$):δ 1.18–1.22 (m, 6H), 1.65 (m, 4H), 1.97–2.11 (m, 4H), 2.36–2.40 (t, 2H), 2.67–2.74 (m, 4H), 2.83–2.87 (t, 2H), 4.0–4.14 (m, 4H), 4.34–4.40 (m, 1H, Gluα-CH), 6.26–6.27 (d, 1H, $J$ = 3.6 Hz), 6.45 (s, 2H, 2-$NH_2$ exch), 6.80 (s, 1H), 7.06–7.07 (d, 1H, $J$ = 3.6 Hz), 8.43–8.45 (d, 1H, $J$ = 7.6, CONH exch), 10.81 (s, 1H, 3-

NH exch). This compound was used directly for next reaction without further purification.

**Diethyl (4-(3-(2-amino-4-oxo-3,4-dihydrothieno [2,3-*d*] pyrimidin-6-yl)propyl)thiophene-2-carbonyl)-L-glutamate (18d).** The general method described for the preparation of target compounds from compound **17d** (0.33 g, 0.98 mmol) was used to prepare **18d** as a yellow semi-solid. Without any further purification step, the glutamate ester **18d** was used for the next reaction.

**Diethyl (4-(4-(2-amino-4-oxo-3,4-dihydrothieno [2,3-*d*] pyrimidin-6-yl)butyl)thiophene-2-carbonyl)-L-glutamate (18e).** The general method described for the preparation of target compounds from compound **17e** (0.36 g, 0.94 mmol) was used to prepare **18e** as a yellow semi-solid. Without any further purification step, the glutamate ester **18e** was used directly for the next reaction.

**Diethyl (5-(3-(2-amino-4-oxo-3,4-dihydrothieno [2,3-*d*] pyrimidin-6-yl)propyl)thiophene-3-carbonyl)-L-glutamate (18f).** The general method described for the preparation of target compounds from compound **17f** (0.39 g, 1.16 mmol) was used to prepare **18f** as a yellow semi-solid. Without any further purification step, the glutamate ester **18f** was used for the next reaction.

**Diethyl (5-(4-(2-amino-4-oxo-3,4-dihydrothieno [2,3-*d*] pyrimidin-6-yl)butyl)thiophene-3-carbonyl)-L-glutamate (18g).** The general method described for the preparation of target compounds from compound **17 g** (0.36 g, 1.03 mmol) was used to prepare **18g** as a yellow semi-solid. Without any further purification step, the glutamate ester **18 g** was used for the next reaction.

*6.2.9. General procedure for the synthesis of target compounds 3–9.*

To a solution of **18** in ethanol (5–10 mL) was added aqueous 1 N NaOH, and the reaction mixture stirred at room temperature for 3 h. The ethanol was evaporated under reduced pressure, and the residue was dissolved in water (5–10 mL). The solution was cooled to 0 ℃ and carefully acidified to pH 3 with dropwise addition of 1 N HCl. The resulting suspension was left at 0 ℃ for 10 min, and the residue was collected by filtration, washed with water (5 mL), and dried over $P_2O_5$/ vacuum at 50 ℃ to afford the free acids **3**–**9.**

**(5-(4-(2-amino-4-oxo-3,4-dihydrothieno [2,3-*d*] pyrimidin-6-yl) butyl)thiophene-2-carbonyl)-L-glutamic acid (3).** The general method described for the preparation of target compounds from compound **18b** was used to prepare final compound **3** as a brown solid (0.22 g, 91%); TLC $R_f$ 0.33 (Methanol/Chloroform = 1:6 + 1 drop of gl. HOAc).mp113.6–114 °C. $^1$H NMR (500 MHz, DMSO-$d_6$): δ 1.97 – 1.86 (m, 2H, $CH_2$), δ 2.07 (dd, 2H, $CH_2$), 2.34 (t, $J$ = 7.5 Hz, 2H), 2.74 (t, $J$ = 6.7 Hz, 2H), 2.83 (d, $J$ = 7.0 Hz, 2H), 4.37–4.30 (m, 1H, CH), 6.49 (s, 2H, $CH_2$), 6.81 (s, 1H, CH, Ar), 6.89 (d, $J$ = 3.7 Hz, 1H, CH, Ar), 7.68 (d, $J$ = 3.7 Hz, 1H, CH, Ar), 8.53 (d, $J$ = 7.8 Hz, 1H, CH, NH), 10.86 (s, 1H, NH). Anal. Calcd for $C_{20}H_{22}N_4O_6S_2 \cdot 1.0\ H_2O$: C, 48.38; H, 4.87; N, 11.28; S, 12.91. Found C, 48.40; H, 4.92; N, 11.12; S, 12.76.

**(5-(4-(2-amino-4-oxo-3,4-dihydrothieno [2,3-*d*] pyrimidin-6-yl) butyl)furan-2-carbonyl)-L-glutamic acid (4).** The general method described for the preparation of target compounds from compound **18c** (0.28 g, 0.57 mmol) was used to prepare final compound **4** as a brown solid (0.23 g, 92%); mp 224.7–225.6 °C; TLC $R_f$ 0.30 (Methanol/Chloroform = 1:6 + 1 drop of gl. HOAc).[1] $^1$H NMR (DMSO-$d_6$): δ1.67 (m, 4H), 1.92–1.94 (m, 2H), 2.08–2.09 (m, 2H), 2.31–2.33 (m, 2H), 2.67–2.74 (m, 2H), 4.32–4.35 (m, 1H, Gluα-CH), 6.28 (d, 1H, $J$ = 3.6 Hz), 6.47 (s, 2H, 2- $NH_2$ exch), 6.82 (s, 1H), 7.06–7.07 (d, 1H, $J$ = 3.6 Hz), 8.31–8.33 (d, 1H, $J$ = 7.6, CONH exch),10.84 (s, 1H, 3-NH exch), 12.55 (br, 2H, 2 COOH); Anal. Calcd for $C_{20}H_{22}N_4O_7S \cdot 0.50\ H_2O$: C, 50.95; H, 4.92; N, 11.88; S, 6.80. Found C, 50.94; H, 4.74; N, 11.73; S, 7.10.

**(5-(3-(2-amino-4-oxo-3,4-dihydrothieno [2,3-*d*] pyrimidin-6-yl) propyl)thiophene-2-carbonyl)-L-glutamic acid (5).** The general method described for the preparation of target compounds from compound **18a** was used to prepare final compound **5** as a brown solid (0.18 g, 92%), mp 147–148 °C; TLC $R_f$ 0.34 (Methanol/Chloroform = 1:6 + 1

drop of gl. HOAc). $^1$H NMR (500 MHz, DMSO-$d_6$): $\delta$ 1.98–1.87 (m, 2H, $CH_2$), 2.11–2.01 (m, 2H, $CH_2$), 2.33 (t, $J = 7.6$ Hz, 2H), 2.75 (t, $J = 7.1$ Hz, 2H, $CH_2$), 2.84 (t, $J = 7.5$ Hz, 2H), 4.33 (dd, $J = 12.8$, 9.6 Hz, 1H), 6.48 (s, 2H, $NH_2$), 6.83 (s, 1H, CH, Ar), 6.92 (d, $J = 3.7$ Hz, 1H, CH, Ar), 7.70 (d, $J = 3.7$ Hz, 1H, CH, Ar), 8.52 (d, $J = 7.6$ Hz, 1H, NH), 10.86 (s, 1H, NH), 12.48 (br, 2H, 2 COOH). Anal. Calcd for $C_{19}H_{20}N_4O_6S_2 \cdot 1.0\ H_2O$: C, 47.29; H, 4.60; N, 11.61; S, 13.29. Found C, 47.20; H, 4.58; N, 11.61; S, 13.20.

**(4-(3-(2-amino-4-oxo-3,4-dihydrothieno [2,3-*d*] pyrimidin-6-yl) propyl)thiophene-2-carbonyl)-L-glutamic acid (6).** The general method described for the preparation of target compounds from compound **18d** was used to prepare final compound **6** as a brown solid (0.145 g, 32% over two steps); mp138 – 139 °C; TLC $R_f$ 0.30 (Methanol/Chloroform = 1:6 + 1 drop of gl. HOAc). $^1$H NMR (500 MHz, DMSO-$d_6$): $\delta$ 1.96–1.87 (m, 2H, $CH_2$), 2.07 (m, 2H, $CH_2$), 2.35 (t, $J = 7.5$ Hz, 2H, $CH_2$), 2.66 – 2.61 (m, 2H, $CH_2$), 2.75 (t, $J = 7.4$ Hz, 2H), 4.37–4.31 (m, 1H, CH), 6.49 (s, 2H, $NH_2$), 6.85 (s, 1H, Ar), 7.44 (s, 1H, Ar), 7.77 (d, $J = 1.1$ Hz, 1H, Ar), 8.55 (d, $J = 7.7$ Hz, 1H, Ar), 10.87 (s, 1H,NH), 12.48 (s, 2H,COOH). Anal. Calcd for $C_{19}H_{20}N_4O_6S_2 \cdot 1.0\ H_2O$: C, 47.29; H, 4.60; N, 11.61; S, 13.29. Found C, 47.22; H, 4.59; N, 11.44; S, 13.21.

**(5-(3-(2-amino-4-oxo-3,4-dihydrothieno [2,3-*d*] pyrimidin-6-yl) propyl)thiophene-3-carbonyl)-L-glu-tamic acid (7).** The general method described for the preparation of target compounds from compound **18f** was used to prepare final compound **7** as a light yellow solid (0.177 g, 35% over two steps), TLC $R_f$ 0(Methanol/Chloroform = 1:5), mp 129.8–131.2 °C. $^1$H NMR (500 MHz, DMSO-$d_6$) :$\delta$ 2.00 – 1.87 (m, 4H, 2$CH_2$), 2.34 (t, $J = 7.5$ Hz, 2H, $CH_2$), 2.80–2.75 (t, 2H, $CH_2$), 2.87–2.81 (t, 2H, $CH_2$), 4.35 (m, 1H, CH), 6.50 (s, 2H, $NH_2$), 6.86 (s, 1H, CH, Ar),7.30 (d, 1H, CH, Ar), 7.99 (d, 1H, CH, Ar), 8.36 (d, $J = 7.7$ Hz, 1H, NH), 10.88 (s,1H,NH), 12.31–12.46 (bs, 2H, 2COOH). Anal. Calcd for $C_{19}H_{20}N_4O_6S_2 \cdot 1.0\ H_2O$: C, 47.29; H, 4.60; N, 11.61; S, 13.29. Found C, 47.47; H, 4.50; N, 11.75; S, 13.45.

**(5-(4-(2-amino-4-oxo-3,4-dihydrothieno [2,3-*d*] pyrimidin-6-yl) butyl)thiophene-3-carbonyl)-L-glutamic acid (8).** The general method described for the preparation of target compounds from compound **18 g** was used to prepare final compound **8** as a light yellow solid (0.198 g, 40% over two steps), mp 138.0–140.0 °C. *Rf* 0.28 (Methanol/Chloroform = 1:6 + 1 drop of gl. HOAc). $^1$H NMR (500 MHz, DMSO-$d_6$): $\delta$1.99–1.88 (m, 4H, 2$CH_2$), 2.11–2.02 (m, 2H, $CH_2$), 2.06 (m, 2H, $CH_2$), 2.34(t, $J = 7.5$ Hz, 2H, $CH_2$), 2.72(t, $J = 7.4$ Hz, 2H, $CH_2$), 2.81 (t, 2H, $CH_2$), 4.35(m, 1H, CH), 6.54(s, 2H, $NH_2$), 6.82 (s,1H, CH, Ar), 7.30 (d, 1H, $J = 1.4$ Hz, CH, Ar), 7.99 (d, $J = 1.4$ Hz, 1H, CH, Ar), 8.36 (d, $J = 7.9$ Hz, 1H, NH),10.92 (s, 1H, NH), 12.33 (bs, 2H, 2COOH). Anal. Calcd for $C_{20}H_{22}N_4O_6S_2 \cdot 1.0$ EtOH: C, 50.37; H, 5.38; N, 10.68; S, 12.22. Found C, 50.40; H, 5.26; N, 10.86; S, 12.15.

**(4-(4-(2-amino-4-oxo-3,4-dihydrothieno [2,3-*d*] pyrimidin-6-yl) butyl)thiophene-2-carbonyl)-L-glutamic acid (9).** The general method described for the preparation of target compounds from compound **18e** was used to prepare final compound **9** as a light yellow solid (0.1474 g, 38% over two steps), mp 104–106 °C. TLC $R_f$ 0.33 (Methanol/Chloroform = 1:6 + 1 drop of gl. HOAc) .$^1$H NMR (500 MHz, DMSO-$d_6$): $\delta$ 1.64(m, 4H, 2$CH_2$), 1.91–2.08(m, 2H, $CH_2$), 2.35 (t, $J = 7.5$ Hz, 2H, $CH_2$), 2.66 – 2.61 (m, 2H, $CH_2$), 2.75 (t, $J = 7.4$ Hz, 2H), 4.37 – 4.31 (m, 1H, CH), 6.47 (s, 2H, $NH_2$), 6.82(s, 1H, Ar), 7.41 (s, 1H, Ar), 7.775 (d, $J = 1.1$ Hz, 1H, Ar), 8.57 (d, $J = 7.9$ Hz, 1H, NH), 10.85 (s, 1H,NH), 12.48 (s, 2H, COOH). Anal. Calcd for $C_{20}H_{22}N_4O_6S_2 \cdot 1.5\ H_2O$: C, 47.52; H, 4.98; N, 11.08; S, 12.68. Found C, 47.21; H, 4.88; N, 10.88; S, 12.42.

### 6.3. Molecular modeling and computational studies

The crystal structure derived from the RCSB was first prepared using the standard protein preparation wizard within the Maestro interface. Three-dimensional (3D) geometries of ligands were generated using LigPrep[53] to provide the energy minimized conformations. Ligands were docked within a box similar to the workspace ligand around the crystallographic binding poses of the co-crystallized ligands. Re-docking was performed in the extended precision mode. Each ligand was re-docked into its corresponding low energy protein structures, and the resulting complexes were ranked according to the docking scores. The top-scoring 20 binding modes were saved for each compound and analyzed visually. From the obtained induced-fit docking results, one pose (ligand − receptor complex) was selected as input structure based on low/minimal MMGBSA docking scores (Schrödinger LLC)[53] and the best poses of the ligand based on the docked scores (the lowest energies in kcal/mol were utilized).

### 6.4. Reagents for biological studies

[3′, 5′, 7, 9-$^3$H] Folic acid (25 Ci/mmol) was purchased from Moravek Biochemicals (Brea, CA). Folic acid was purchased from Sigma Chemical Co. (St.Louis, MO). Leucovorin [(6R,S) 5-formyl tetrahydrofolate] and MTX were provided by the Drug Development Branch, National Cancer Institute (Bethesda, MD). PMX [N-{4-[2- (2-amino-3,4-dihydro-4-oxo-7H-pyrrolo[2,3-*d*]pyrimidin-5-yl)ethyl]benzoyl-L-glutamic acid] (Alimta) was purchased from LC Laboratories (Woburn, MA). The syntheses of **AGF23** and **AGF94** were previously described.[7,36] Additional chemicals were purchased from commercial sources in the highest available purities.

### 6.5. Cell Culture

The RFC-, PCFT- and FRα-null CHO cell line MTXRIIOua$^R$2-4 was a generous gift from Dr. Wayne Flintoff (University of Western Ontario).[54] Four sublines were derived from the R2 line by transfection with either RFC, PCFT, FRα, or FRβ to give rise to PC43-10 (expresses only human RFC), R2/PCFT4 (expresses only human PCFT), RT16 (expresses only human FRα), and D4 (expresses only human FRβ).[7,40,56] Isogenic CHO sublines were cultured in α-minimal essential medium (α-MEM) supplemented with 100 units/mL penicillin/100 μg/mL streptomycin, 2 mM L-glutamine and 10% bovine calf serum (Sigma-Aldrich). Transfected sublines of R2 cells were maintained in the presence of 1.5 mg/ml G418. Prior to cell viability assays, RT16 and D4 CHO cells were cultured in folate-free RPMI 1640 (FF-RPMI) (Invitrogen) with dialyzed fetal bovine serum (Invitrogen), supplemented with 100 units/mL penicillin/100 μg/mL streptomycin, and 2 mM L-glutamine.

Mammalian FRα-expressing KB nasopharyngeal carcinoma cells were obtained from the American Type Culture Collection (Manassas, VA) and IGROV1 (NCI-IGROV1) (passage 5) clear cell carcinoma cells[57] were obtained from the Division of Cancer Treatment and Diagnosis, National Cancer Institute (Frederick, MD). NCI-IGROV1 and KB cells were cultured in complete FF-RPMI supplemented with 10% fetal bovine serum and 100 units/mL penicillin/100 μg/mL streptomycin, and 2 mM L-glutamine. Cell proliferation assays were performed as previously described.[7,15] CHO, KB and NCI-IGROV1 cells were plated in 96-well dishes at densities ranging from 2500 to 5000 cells/well in 200 μL media and treated with a range of inhibitors spanning 0–1000 nM. Experiments with RT16, D4, NCI-IGROV1 and KB cells used FF RPMI media with 10% dialyzed FBS and 100 units/mL penicillin/100 μg/mL streptomycin, supplemented with 2 nM leucovorin and 2 mM L-glutamine. FR-mediated drug uptake was assessed in parallel incubations including 200 nM folic acid. For R2/PCFT4, PC43-10 and R2 CHO cells, the medium was FF-RPMI supplemented with 10% dialyzed FBS, 100 units/mL penicillin/100 μg/mL streptomycin, 25 nM leucovorin and 2 mM L-glutamine. Cells were treated over a 96 h period at 37° C with 5% $CO_2$ and relative cell numbers quantified using the CellTiter-blue cell viability assay (Promega, Madison, WI) and a fluorescence plate reader.[7] Raw data were exported to Excel for analysis and the results plotted using Graphpad Prism 6.0. Determinations of $IC_{50}$s were made corresponding to the drug concentrations that resulted in 50% loss of cell growth.

Using KB cells, proliferation assays were performed with nucleoside/AICA rescue to identify the targeted pathway and enzyme(s).[34,40]

Inhibitory effects of the novel analogs on *de novo* thymidylate biosynthesis and *de novo* purine nucleotide biosynthesis were tested by incubating drugs with thymidine (10 μM) and adenosine (60 μM), respectively. To distinguish targeting between the folate-dependent purine biosynthetic enzymes GARFTase and AICARFTase, co-incubation experiments were performed using AICA hydrochloride (320 μM).[34,40]

### 6.6. FR binding assay

Relative binding affinities of novel C1 inhibitors to FRα and FRβ were determined through a competitive binding assay with [$^3$H]folic acid.[7] FRα- and FRβ-expressing RT16 and D4 CHO cells, respectively, were plated at a density of $1 \times 10^6$ cells in complete α-MEM media. Cells were allowed to adhere to the plates for 24 h. The cells were washed with 4 °C Dulbecco's phosphate-buffered saline (DPBS), followed by acetate buffer (10 mM sodium acetate, 150 mM NaCl, pH 3.5) at 4 °C to release FRα-bound folates, then neutralized with Hepes-buffered saline (HBS) (20 mM Hepes, 140 mM NaCl, 5 mM KCl, 2 nM $MgCl_2$, and 5 mM glucose, pH 7.4) at 4 °C. Following the washes, cells were incubated at 0 °C for 15 min with [$^3$H]folic acid (50 nM, specific activity 0.5 Ci/mmol), without or with unlabeled folic acid (positive control), MTX (negative control) or the novel C1 inhibitors over a range of concentrations. After a 15 min incubation, the cells were washed with ice-cold HBS and proteins were solubilized with 0.5 N NaOH. Protein concentrations were measured using Folin-phenol reagent.[63] Cell homogenates were assayed for radioactivity with a liquid scintillation counter. Calculations of [$^3$H]folic acid bound to FRs were calculated as pmol [$^3$H]folic acid/mg protein; relative binding affinities were calculated as the inverse molar ratios of unlabeled ligand needed to inhibit [$^3$H]folic acid binding to FRs by 50%. Unlabeled folic acid as a competitor in this assay was assigned a relative affinity of 1 for comparison.

### 6.7. In vitro targeted metabolomics

NCI-IGROV1 EOCs were seeded in five replicate 60 mm dishes in FF RPMI supplemented with 10% fetal bovine serum, 1% penicillin/streptomycin, and 2 mM L-glutamine. Cells were allowed to adhere for 24 h. The media was aspirated and replaced, and 1 μM inhibitor or a comparable volume of DMSO (vehicle) was added. Cells were incubated with inhibitor for 48 h. Metabolites were extracted[4] and normalized to total cell protein from the post-extraction pellet (solubilized in 0.5 N NaOH) using the Folin-phenol method.[63] NCI-IGROV1 vehicle and drug-treated samples were analyzed on a ThermoElectron Corporation Exactive mass spectrometer in negative ion mode. Samples were separated on a reverse phase Atlantis T3, 100 mm X 3 μM column (Waters). Metabolites were identified by their exact masses and retention times were compared against the retention times of standard metabolites using MultiQuant 3.0.1 software.

### 6.8. Enzyme expression and purification

The *N*-terminal His-tagged human GARFTase formyltransferase domain and *N*-terminal His-tagged full-length human AICARFTase/IMP cyclohydrolase (ATIC) were expressed and purified as previously described using Ni-NTA immobilized metal affinity and size exclusion chromatography.[4,50]

### 6.9. In vitro enzymatic assays and $K_i$ determinations

AICARFTase catalytic activity was measured by monitoring the formation of tetrahydrofolate from 10-formyl tetrahydrofolate (10-CHO-THF) in the presence of a range of inhibitor concentrations.[64] Reactions were carried out at final concentrations of 50 μM 10-CHO-THF, 100 nM His-ATIC, 50 μM ZMP, and inhibitors in 32.6 mM Tris-HCl, pH 7.5, 25 mM KCl, and 5 mM β-mercaptoethanol.[4] GARFTase catalytic activity was measured by monitoring the formation of THF from 10-CHO-THF in the presence of inhibitor. GARFTase assays included final concentrations of 40 μM 10-CHO-THF, 50 nM His-GARFTase, 15 μM α,β-GAR, and a range of inhibitor concentrations in 25 mM Tris-HCl pH 8.0, 300 mM NaCl, and 5 mM β-mercaptoethanol.[4] Kinetic measurements were recorded in triplicate in a UV-transparent 96-well plate (Costar 3635) at 298 nm using a BioTek Synergy Neo2 Plate Reader. Initial slopes were graphed against inhibitor concentrations and fit to a three-parameter nonlinear regression to calculate the $IC_{50}$ for each compound (GraphPad Prism 8.0). $K_i$ values were calculated from the $IC_{50}$, [$K_i = IC_{50}/([10\text{-CHO-THF}]/K_M + 1)$], using previously determined $K_M$ values of 10-CHO-THF with His-ATIC or His-GARFTase of 100 μM and 84.8 μM, respectively.

### 6.10. Crystallization of human GARFTase, X-ray data collection and structure determination

The GAR formyltransferase domain of the trifunctional purine biosynthetic protein adenosine-3 (residues 808–1010), engineered with a non-cleavable C-terminal hexahistidine tag (GARFTase-His), was buffer-exchanged into 25 mM Tris-HCl pH 8.0, 200 mM NaCl, 0.6 mM Tris(2-carboxyethyl)phosphine (TCEP) and concentrated to 10 mg/mL. GARFTase-His was incubated at 4 °C for 30 min in a 3-fold molar ratio with α,β-GAR in excess, in the presence or absence of inhibitors (stock solution dissolved in DMSO) before crystallization screens were set up and incubated at 4 °C. Hanging drop plates contained 1 μL of protein–ligand solution, 0.8 μL of crystal condition, and 0.2 μL of 9 mM *N*-decyl β-D-thiomaltoside (Hampton Research, Aliso Viejo, CA) equilibrated over 0.5 mL of crystallant consisting of 0.1 M Tris-HCl pH 7.5, 0.33 M NaCl, 16–21% polyethylene glycol (PEG) 4000, and 2% PEG 400. Cube-shaped crystals formed within a few days and were frozen by direct immersion in liquid nitrogen after being transferred stepwise to crystallant with 35% PEG 4000. In some cases, the inhibitors were soaked into GARFTase-His/α,β-GAR complex crystals. For these experiments, crystals were transferred to cryoprotectant and allowed to soak in a 3:3:1 α,β-GAR:inhibitor:GARFTase-His molar ratio for at least 30 min prior to flash freezing.

Data collection was performed at Lawrence Berkeley National Laboratory Advanced Light Source beamline 4.2.2 using the Taurus CMOS detector. All data sets were processed in space group $P3_22$ (XDS[65-67]). Molecular replacement was performed using Protein Data Bank (PDB) entry 1J9F with waters and ligands removed as a search model (PHENIX[68]). Subsequent model building and refinement were performed using Coot[69] and PHENIX[68], respectively.

### 6.11. Statistical analysis

Data were checked for their distributional assumptions and, if needed, were transformed to meet the normality assumption. Statistical comparisons were performed using two-sided, unpaired t-tests after log-transformation. Multiple comparisons correction was implemented using a Holm's procedure. For metabolomics analyses, concentrations were transformed toward normality using a square-root transformation. Statistical analyses were carried out using R and GraphPad Prism.

## Declaration of Competing Interest

The authors declare that they have no known competing financial interests or personal relationships that could have appeared to influence the work reported in this paper.

*Acknowledgements*

This work was supported in part by grants from the National Institutes of Health R01 CA53535 (LHM and ZH), R01 CA125153 (AG), R01 CA152316 (LHM and AG), R01 CA166711 (AG, LHM and CED), and

R01 GM094472 (CED), a Metabolomics Pilot Grant from the Karmanos Cancer Institute, the Eunice and Milton Ring Endowed Chair for Cancer Research (LHM), and the Duquesne University Adrian Van Kaam Chair in Scholarly Excellence (AG). Ms. Wallace-Povirk was supported by T32 CA009531 (LHM) and F31 CA243215-01. We thank T.S. Widlanski for providing the α, β-GAR substrate for crystallography and enzyme inhibition experiments. All GARFTase crystallization experiments were carried out in the Indiana University METACyt Crystallization Automation Facility. This research used resources of the Advanced Photon Source, a U.S. Department of Energy (DOE) Office of Science User Facility operated for the DOE Office of Science by Argonne National Laboratory under Contract No. DE-AC02-06CH11357. The Biostatistics and Bioinformatics Core (S. Kim) and the Pharmacology and Metabolomics Core (X. Bao, J. Li) were supported, in part, by NIH Center grant P30 CA022453 to the Barbara Ann Karmanos Cancer Institute and the Wayne State University.

## Appendix A. Supplementary data

Supplementary data to this article can be found online at https://doi.org/10.1016/j.bmc.2021.116093.

## References

1 Lucock M. Folic acid: nutritional biochemistry, molecular biology, and role in disease processes. *Mol Genet Metab*. 2000;71:121–138.
2 Stover PJ. Physiology of folate and vitamin B12 in health and disease. *Nutr Rev*. 2004;62:S3–S12. discussion S13.
3 Yu W, Wang Z, Zhang K, et al. One-Carbon Metabolism Supports S-Adenosylmethionine and Histone Methylation to Drive Inflammatory Macrophages. *Mol Cell*. 2019;75(1147–1160), e5.
4 Dekhne AS, Shah K, Ducker GS, et al. Novel pyrrolo[3,2-d]pyrimidine compounds target mitochondrial and cytosolic one-carbon metabolism with broad-spectrum antitumor efficacy. *Mol Cancer Ther*. 2019;18:1787–1799.
5 Ducker GS, Chen L, Morscher RJ, et al. Reversal of Cytosolic One-Carbon Flux Compensates for Loss of the Mitochondrial Folate Pathway. *Cell Metab*. 2016;23:1140–1153.
6 Dekhne AS, Hou Z, Gangjee A, Matherly LH. Therapeutic Targeting of Mitochondrial One-Carbon Metabolism in Cancer. *Mol Cancer Ther*. 2020;19:2245–2255.
7 Deng Y, Wang Y, Cherian C, et al. Synthesis and discovery of high affinity folate receptor-specific glycinamide ribonucleotide formyltransferase inhibitors with antitumor activity. *J Med Chem*. 2008;51:5052–5063.
8 Visentin M, Zhao R, Goldman ID. The antifolates. *Hematol Oncol Clin North Am*. 2012;26:629–648.
9 Goldman ID, Matherly LH. The cellular pharmacology of methotrexate. *Pharmacol Ther*. 1985;28:77–102.
10 Chattopadhyay S, Moran RG, Goldman ID. Pemetrexed: biochemical and cellular pharmacology, mechanisms, and clinical applications. *Mol Cancer Ther*. 2007;6:404–417.
11 Zhao R, Goldman ID. Resistance to antifolates. *Oncogene*. 2003;22:7431–7457.
12 Matherly LH, Hou Z, Deng Y. Human reduced folate carrier: translation of basic biology to cancer etiology and therapy. *Cancer metastasis reviews*. 2007;26:111–128.
13 Zhao R, Goldman ID. The molecular identity and characterization of a Proton-coupled Folate Transporter–PCFT; biological ramifications and impact on the activity of pemetrexed. *Cancer metastasis reviews*. 2007;26:129–139.
14 Zhao R, Matherly LH, Goldman ID. Membrane transporters and folate homeostasis: intestinal absorption and transport into systemic compartments and tissues. *Expert Rev Mol Med*. 2009;11, e4.
15 Hou Z, Gattoc L, O'Connor C, et al. Dual targeting of epithelial ovarian cancer via folate receptor alpha and the proton-coupled folate transporter with 6-substituted pyrrolo[2,3-d]pyrimidine antifolates. *Mol Cancer Ther*. 2017;16:819–830.
16 Hou Z, Matherly LH. Biology of the Major Facilitative Folate Transporters SLC19A1 and SLC46A1. *Curr Top Membr*. 2014;73:175–204.
17 Wilson MR, Hou Z, Yang S, et al. Targeting Nonsquamous Nonsmall Cell Lung Cancer via the Proton-Coupled Folate Transporter with 6-Substituted Pyrrolo[2,3-d] Pyrimidine Thienoyl Antifolates. *Mol Pharmacol*. 2016;89:425–434.
18 Kugel Desmoulin S, Wang L, Hales E, et al. Therapeutic targeting of a novel 6-substituted pyrrolo [2,3-d]pyrimidine thienoyl antifolate to human solid tumors based on selective uptake by the proton-coupled folate transporter. *Mol Pharmacol*. 2011;80:1096–1107.
19 Giovannetti E, Zucali PA, Assaraf YG, et al. Role of proton-coupled folate transporter in pemetrexed resistance of mesothelioma: clinical evidence and new pharmacological tools. *Ann Oncol*. 2017;28:2725–2732.
20 Jackman, A. L.; Jackman, A. L.; Leamon, C. P., Targeted drug strategies for cancer and inflammation. Springer,: New York, 2011; p 1 online resource (261 p.).
21 Elnakat H, Ratnam M. Distribution, functionality and gene regulation of folate receptor isoforms: implications in targeted therapy. *Adv Drug Deliv Rev*. 2004;56:1067–1084.
22 Puig-Kroger A, Sierra-Filardi E, Dominguez-Soto A, et al. Folate receptor beta is expressed by tumor-associated macrophages and constitutes a marker for M2 anti-inflammatory/regulatory macrophages. *Cancer Res*. 2009;69:9395–9403.
23 Nunez MI, Behrens C, Woods DM, et al. Wistuba, II, High expression of folate receptor alpha in lung cancer correlates with adenocarcinoma histology and EGFR [corrected] mutation. *J Thorac Oncol*. 2012;7:833–840.
24 Parker N, Turk MJ, Westrick E, Lewis JD, Low PS, Leamon CP. Folate receptor expression in carcinomas and normal tissues determined by a quantitative radioligand binding assay. *Anal Biochem*. 2005;338:284–293.
25 Weitman SD, Lark RH, Coney LR, et al. Distribution of the folate receptor GP38 in normal and malignant cell lines and tissues. *Cancer Res*. 1992;52:3396–3401.
26 Kamen BA, Smith AK. Farletuzumab, an anti-folate receptor alpha antibody, does not block binding of folate or anti-folates to receptor nor does it alter the potency of anti-folates in vitro. *Cancer Chemother Pharmacol*. 2012;70:113–120.
27 Kurkjian C, LoRusso P, Sankhala KK, et al. A phase I, first-in-human studyto evaluate the safety, pharmacokinetics (PK), and pharmacodynamics (PD) ofIMGN853 in patients (Pts) with epithelial ovarian cancer (EOC) and other FOLR1-positive solid tumors. *J. Clin. Oncol.* 2013;31:2573.
28 Assaraf YG, Leamon CP, Reddy JA. The folate receptor as a rational therapeutic target for personalized cancer treatment. *Drug Resist Updat*. 2014;17:89–95.
29 Banerji U, Garces AHI, Michalarea V, et al. An investigator-initiated phase I study of ONX-0801, a first-in-class alpha folate receptor targeted, small molecule thymidylate synthase inhibitor in solid tumors. *J Clin Oncol*. 2017;35:2503.
30 O'Malley DM, Matulonis UA, Birrer MJ, et al. Mirvetuximab soravtansine, a folate receptor alpha (FRα)-targeting antibody-drug conjugate (ADC), in combination with bevacizumab in patients (pts) with platinum-resistant ovarian cancer: Final findings from the FORWARD II study. *J Clin Oncol*. 2019;37:5520.
31 Matherly, L. H.; Wilson, M. R.; Hou, Z., The Major Facilitative Folate Transporters SLC19A1 and SLC46A1: Biology and Role in Antifolate Chemotherapy of Cancer. Drug metabolism and disposition: the biological fate of chemicals 2014.
32 Rothbart SB, Racanelli AC, Moran RG. Pemetrexed indirectly activates the metabolic kinase AMPK in human carcinomas. *Cancer Res*. 2010;70:10299–10309.
33 Golani LK, Islam F, O'Connor C, et al. Design, synthesis and biological evaluation of novel pyrrolo[2,3-d]pyrimidine as tumor-targeting agents with selectivity for tumor uptake by high affinity folate receptors over the reduced folate carrier. *Bioorg Med Chem*. 2020;28(12), 115544.
34 Mitchell-Ryan S, Wang Y, Raghavan S, et al. Discovery of 5-substituted pyrrolo[2,3-d]pyrimidine antifolates as dual acting inhibitors of glycinamide ribonucleotide formyltransferase and 5-aminoimidazole-4-carboxamide ribonucleotide formyltransferase in de novo purine nucleotide biosynthesis: implications of inhibiting 5-aminoimidazole-4-carboxamide ribonucleotide formyltransferase to AMPK activation and anti-tumor activity. *J Med Chem*. 2013;56:10016–10032.
35 Wang L, Cherian C, Desmoulin SK, et al. Synthesis and antitumor activity of a novel series of 6-substituted pyrrolo[2,3-d]pyrimidine thienoyl antifolate inhibitors of purine biosynthesis with selectivity for high affinity folate receptors and the proton-coupled folate transporter over the reduced folate carrier for cellular entry. *J Med Chem*. 2010;53:1306–1318.
36 Wang L, Desmoulin SK, Cherian C, et al. Synthesis, biological, and antitumor activity of a highly potent 6-substituted pyrrolo[2,3-d]pyrimidine thienoyl antifolate inhibitor with proton-coupled folate transporter and folate receptor selectivity over the reduced folate carrier that inhibits beta-glycinamide ribonucleotide formyltransferase. *J Med Chem*. 2011;54:7150–7164.
37 Wang L, Wallace A, Raghavan S, et al. 6-Substituted Pyrrolo[2,3-d]pyrimidine Thienoyl Regioisomers as Targeted Antifolates for Folate Receptor alpha and the Proton-Coupled Folate Transporter in Human Tumors. *J Med Chem*. 2015;58:6938–6959.
38 Ravindra M, Wilson MR, Tong N, et al. Fluorine-Substituted Pyrrolo[2,3-d] Pyrimidine Analogues with Tumor Targeting via Cellular Uptake by Folate Receptor α and the Proton-Coupled Folate Transporter and Inhibition of de Novo Purine Nucleotide Biosynthesis. *J Med Chem*. 2018;61(9):4228–4248.
39 Ravindra M, Wallace-Povirk A, Karim MA, et al. Tumor Targeting with Novel Pyridyl 6-Substituted Pyrrolo[2,3- d]Pyrimidine Antifolates via Cellular Uptake by Folate Receptor alpha and the Proton-Coupled Folate Transporter and Inhibition of De Novo Purine Nucleotide Biosynthesis. *J Med Chem*. 2018;61:2027–2040.
40 Deng Y, Zhou X, Kugel Desmoulin S, et al. Synthesis and biological activity of a novel series of 6-substituted thieno[2,3-d]pyrimidine antifolate inhibitors of purine biosynthesis with selectivity for high affinity folate receptors over the reduced folate carrier and proton-coupled folate transporter for cellular entry. *J Med Chem*. 2009;52:2940–2951.
41 Petrelli A, Giordano S. From single- to multi-target drugs in cancer therapy: when aspecificity becomes an advantage. *Curr Med Chem*. 2008;15:422–432.
42 Wang, X. Z., H.; Chen, X. , Drug resistance and combating drug resistance in cancer Cancer Drug Resistance 2019, 2, 141-160.
43 Brunetti L, Loiodice F, Piemontese L, Tortorella P, Laghezza A. New Approaches to Cancer Therapy: Combining Fatty Acid Amide Hydrolase (FAAH) Inhibition with Peroxisome Proliferator-Activated Receptors (PPARs) Activation. *J Med Chem*. 2019;62:10995–11003.
44 Martinez R, Geronimo BD, Pastor M, et al. Multitarget Anticancer Agents Based on Histone Deacetylase and Protein Kinase CK2 inhibitors. *Molecules*. 2020;25.
45 Zhou J, Jiang X, He S, et al. Rational Design of Multitarget-Directed Ligands: Strategies and Emerging Paradigms. *J Med Chem*. 2019;62:8881–8914.
46 Antolin AA, Workman P, Mestres J, Al-Lazikani B. Polypharmacology in Precision Oncology: Current Applications and Future Prospects. *Curr Pharm Des*. 2016;22:6935–6945.
47 Zhuang W, Bolognesi M, Seri M, et al. Influence of Incorporating Different Electron-Rich Thiophene-Based Units on the Photovoltaic Properties of Isoindigo-Based

Conjugated Polymers: An Experimental and DFT Study. *Macromolecules*. 2013;46:8488–8499.
48 Golani LK, Wallace-Povirk A, Deis SM, et al. Tumor Targeting with novel 6-substituted pyrrolo [2,3-d]pyrimidine antifolates with heteroatom bridge substitutions via cellular uptake by folate receptor alpha and the proton-coupled folate transporter and inhibition of de novo purine nucleotide biosynthesis. *J Med Chem*. 2016;59:7856–7876.
49 Wibowo AS, Singh M, Reeder KM, et al. Structures of human folate receptors reveal biological trafficking states and diversity in folate and antifolate recognition. *Proc Natl Acad Sci U S A*. 2013;110:15180–15188.
50 Deis SM, Doshi A, Hou Z, et al. Structural and Enzymatic Analysis of Tumor-Targeted Antifolates That Inhibit Glycinamide Ribonucleotide Formyltransferase. *Biochemistry*. 2016;55:4574–4582.
51 Wang L, Wallace A, Raghavan S, et al. 6-Substituted Pyrrolo[2,3-d]pyrimidine Thienoyl Regioisomers as Targeted Antifolates for Folate Receptor α and the Proton-Coupled Folate Transporter in Human Tumors. *J Med Chem*. 2015;58:6938–6959.
52 Cheong CG, Wolan DW, Greasley SE, Horton PA, Beardsley GP, Wilson IA. Crystal structures of human bifunctional enzyme aminoimidazole-4-carboxamide ribonucleotide transformylase/IMP cyclohydrolase in complex with potent sulfonyl-containing antifolates. *J Biol Chem*. 2004;279:18034–18045.
53 Schrödinger Release 2019-2: Maestro, S., LLC: New York, NY, 2019.
54 Flintoff WF, Davidson SV, Siminovitch L. Isolation and partial characterization of three methotrexate-resistant phenotypes from Chinese hamster ovary cells. *Somatic cell genetics*. 1976;2:245–261.
55 Kugel Desmoulin S, Wang Y, Wu J, et al. Targeting the proton-coupled folate transporter for selective delivery of 6-substituted pyrrolo[2,3-d]pyrimidine antifolate inhibitors of de novo purine biosynthesis in the chemotherapy of solid tumors. *Mol Pharmacol*. 2010;78:577–587.
56 Wong SC, Proefke SA, Bhushan A, Matherly LH. Isolation of human cDNAs that restore methotrexate sensitivity and reduced folate carrier activity in methotrexate transport-defective Chinese hamster ovary cells. *J Biol Chem*. 1995;270:17468–17475.
57 Benard J, Da Silva J, De Blois MC, et al. Characterization of a human ovarian adenocarcinoma line, IGROV1, in tissue culture and in nude mice. *Cancer Res*. 1985;45:4970–4979.
58 Pedley AM, Benkovic SJ. A New View into the Regulation of Purine Metabolism: The Purinosome. *Trends Biochem Sci*. 2017;42:141–154.
59 Tong X, Zhao F, Thompson CB. The molecular determinants of de novo nucleotide biosynthesis in cancer cells. *Curr Opin Genet Dev*. 2009;19:32–37.
60 Bronder JL, Moran RG. A defect in the p53 response pathway induced by de novo purine synthesis inhibition. *J Biol Chem*. 2003;278:48861–48871.
61 Bertino JR, Waud WR, Parker WB, Lubin M. Targeting tumors that lack methylthioadenosine phosphorylase (MTAP) activity: current strategies. *Cancer Biol Ther*. 2011;11:627–632.
62 Hoxhaj G, Hughes-Hallett J, Timson RC, et al. The mTORC1 Signaling Network Senses Changes in Cellular Purine Nucleotide Levels. *Cell Rep*. 2017;21:1331–1346.
63 Lowry OH, Rosebrough NJ, Farr AL, Randall RJ. Protein measurement with the Folin phenol reagent. *J Biol Chem*. 1951;193:265–275.
64 Shih C, Chen VJ, Gossett LS, et al. LY231514, a pyrrolo[2,3-d]pyrimidine-based antifolate that inhibits multiple folate-requiring enzymes. *Cancer Res*. 1997;57:1116–1123.
65 Kabsch W. Integration, scaling, space-group assignment and post-refinement. *Acta Crystallogr D Biol Crystallogr*. 2010;66:133–144.
66 Kabsch, W., Xds. Acta Crystallogr D Biol Crystallogr 2010, 66, 125-32.
67 Evans PR, Murshudov GN. How good are my data and what is the resolution? *Acta Crystallogr D Biol Crystallogr*. 2013;69:1204–1214.
68 Adams PD, Afonine PV, Bunkoczi G, et al. PHENIX: a comprehensive Python-based system for macromolecular structure solution. *Acta Crystallogr D Biol Crystallogr*. 2010;66:213–221.
69 Emsley P, Lohkamp B, Scott WG, Cowtan K. Features and development of Coot. *Acta Crystallogr D Biol Crystallogr*. 2010;66:486–501.